Linking Brain Circuitry and Neural Plasticity in Antidepressant Response: The mPFC-Reuniens-Hippocampus Pathway.

Stefan Vestring, Maxime Veleanu, Jakob Weber, Tim Schwär, Louise Schuberth, David Sarrazin, Marguerite Anselin, Lukas Rutke, Guillermo Jose Suarez-Marchi, Stella Zimmermann, et al.

Linking Brain Circuitry and Neural Plasticity in Antidepressant Response: The mPFC-Reuniens-Hippocampus Pathway.

Stefan Vestring

stefan.vestring@uniklinik-freiburg.de

Medical Center - University of Freiburg

Maxime Veleanu

Department of Psychiatry and Psychotherapy, Medical Center - University of Freiburg
https://orcid.org/0000-0001-6760-3488

Jakob Weber

University of Freiburg, Faculty of Medicine, University of Freiburg, Freiburg, Germany

Tim Schwär

University of Freiburg, Faculty of Medicine, University of Freiburg, Freiburg, Germany

Louise Schuberth

University of Freiburg, Faculty of Medicine, University of Freiburg, Freiburg, Germany

David Sarrazin

https://orcid.org/0000-0003-1326-3232

Marguerite Anselin

University of Freiburg, Faculty of Medicine, University of Freiburg, Freiburg, Germany

Lukas Rutke

University of Freiburg, Faculty of Medicine, University of Freiburg, Freiburg, Germany

Guillermo Jose Suarez-Marchi

Medical Center - University of Freiburg https://orcid.org/0009-0005-6219-0174

Stella Zimmermann

Medical Center - University of Freiburg

Zoe Borgeest

University of Freiburg, Faculty of Medicine, University of Freiburg, Freiburg, Germany

Martin Balzinger

Centre National de la Recherche Scientifique (CNRS)

Alina Blendinger

Centre National de la Recherche Scientifique (CNRS) UPR3212, Université de Strasbourg, Institut des Neurosciences Cellulaires et Intégratives (INCI), Strasbourg, France

Anna Catarata

Department for Psychiatry and Psychotherapy, Medical Center – University of Freiburg, Faculty of Medicine, University of Freiburg, Freiburg, Germany.

Samira Assaad Dib
University of Freiburg, Faculty of Medicine, University of Freiburg, Freiburg, Germany

Thibault Cholvin
University of Freiburg, Medical Faculty https://orcid.org/0000-0002-9964-7693

Yaroslav Sych
University of Strasbourg https://orcid.org/0000-0002-1822-8631

Katharina Domschke
University of Freiburg https://orcid.org/0000-0002-2550-9132

Claus Normann
Medical Center - University of Freiburg https://orcid.org/0000-0001-5693-8936

Tsvetan Serchov
University of Strasbourg Institute for Advanced Study (USIAS)

Article

Keywords:

Posted Date: April 3rd, 2025

DOI: https://doi.org/10.21203/rs.3.rs-6348176/v1

Additional Declarations: Yes there is potential Competing Interest. C.N. and K.D. received lecture fees and advisory board honoraria from Johnson & Johnson, the manufacturer of Esketamine. C.N. received research support as a principal investigator in clinical trials sponsored by Johnson & Johnson. C.N. received honoraria as a member of a DMC board by Novartis. T.S. received honoraria consulting Primetime Life Sciences, LLC. All other authors declare that they have no competing interests.

Abstract

The pathophysiology of depression involves multiple biological processes, including circuit dysfunction and impaired neuroplasticity, yet an integrative view that links these processes remains elusive. Here, using a combination of circuit manipulation, electrophysiology, behavior, and fiber photometry, we identify a convergent circuit for antidepressant response and plasticity modulation. We demonstrate that chemogenetic activation of the infralimbic cortex (IL) is sufficient to exert rapid antidepressant effects across multiple behavioral domains in a mouse model of stress-induced depression and exerts top-down control over hippocampal plasticity and processing. We show that IL stimulation enhances structural plasticity, restores long-term potentiation and improves state-dependent network dynamics in the hippocampus (HIP). We identified the nucleus reuniens (RE) as a necessary mediator of these effects. Notably, RE inhibition blocks not only IL stimulation-induced antidepressant response but also the therapeutic and neuroplastic effects of ketamine. Our findings demonstrate that the functional IL → RE → ventral HIP circuit plays a central role in the antidepressant response, linking circuit activity, HIP plasticity, and depressive-like behaviors.

Introduction

Major depressive disorder (MDD) is a widespread and devastating condition that causes immense suffering and heavy socioeconomic burdens[1]. The treatments that are currently available have slow mechanisms of action and can increase suicidal ideation. Additionally, the high proportion of nonresponders among patients who receive these treatments highlights the urgent need for new, fast-acting antidepressants[2].

The discovery of the rapid antidepressant effects of ketamine has challenged the monoaminergic deficits hypothesis of MDD, providing new perspectives that have led to the proposition of alternative frameworks for understanding the pathophysiology of depression and treating this condition[3,4]. For example, the neurocircuit hypothesis postulates that depression might occur due to dysfunctional information processing and connectivity patterns in specific key networks[5], whereas the neuroplasticity hypothesis proposes that an impaired ability to modify synaptic strength and neural connections underlies depressive pathology[6,7]. Correspondingly, stimulation of selected brain circuits and regions or enhancement of synaptic plasticity promotes antidepressant response[8,9]. Despite being extensively studied in humans and animal models, the link or potential interdependence between these two frameworks remains poorly understood.

Neuroimaging studies, postmortem analyses, and preclinical research have indicated that depression is associated with structural and functional deregulations in a subset of brain regions[10–12]. The prefrontal cortex (PFC) has emerged as one of the regions that is most consistently impaired in patients with depression[13], with the most consistent volumetric and structural deficits, such as cortical atrophy or a decrease in synaptic density[14]. More recently, the largest study involving precision functional mapping to

date identified a strong role of the frontostriatal salience network in depression, even allowing for the prediction of the emergence of depressive symptoms[15]. At the preclinical level, multiple studies have demonstrated structural and functional deficits in the medial prefrontal cortex (mPFC) of rodent models of depression, and successful treatments with antidepressant therapies often involve prefrontal mechanisms[16,17]. Therapeutic interventions that impact prefrontal activity, including transcranial magnetic stimulation (TMS)[18], deep brain stimulation (DBS)[9], or treatment with the fast-acting antidepressant ketamine, reverse depressive-like phenotypes. Finally, the mPFC, especially the IL region, is extensively connected to limbic brain structures, such as the nucleus accumbens (NAc) and the ventral tegmental area (VTA), both of which are implicated in the control of reward, motivation and mood[12,19,20]; these findings highlight the role of the mPFC as a central "hub" in depression[21].

Neuroplasticity is the ability of the brain to undergo biological changes in response to a changing environment. Neuroplasticity is thought to play a major role in depression by modulating the brain's response to aversive experiences or chronic stress[22]. Several paradigms that provide indirect readouts of neuroplasticity in humans, such as paired associative stimulation (PAS) and recording motor[23] or visual[24] evoked potentials, revealed a decrease in the correlates of synaptic plasticity in depressed patients, which was reversed by antidepressant therapy. Both structural (synaptic density) and associative plasticity, which are two mechanisms that are crucial for learning, have been extensively studied in the hippocampus (HIP). Rodent models of depression have systematically shown impaired long-term potentiation (LTP)[25,26], and the antidepressant effect of drugs such as ketamine has been associated with the amelioration of LTP deficits in the HIP, suggesting a major role for associative plasticity in MDD and antidepressant response[27]. Despite the abundant evidence supporting major roles of the PFC and the HIP in depression, an integrative investigation linking prefrontal circuits with HIP neuroplasticity in the context of depression treatment is lacking.

In this study, we initially confirmed the potential of mPFC stimulation to elicits antidepressant effects using a chemogenetic approach (designer receptor exclusively activated by designer drugs; DREADDs). Next, we unraveled the downstream circuit mechanisms and showed that the mPFC exerts a top-down control on hippocampal structural plasticity, LTP induction and information processing. Notably, we identified the nucleus reuniens (RE) as a necessary link between the mPFC and HIP for mediating antidepressant and neuroplastic effects of mPFC stimulation and ketamine. Overall, we provide the first evidence for the central role of the mPFC–RE–HIP circuit in the response to antidepressants, acting as a loop controlling HIP plasticity and depressive-like behavior.

Results

Prolonged chemogenetic activation of IL excitatory neurons exerts antidepressant-like effects in various behavioral paradigms

To investigate the role of excitatory neurons in the mPFC, we stereotactically injected an adeno-associated virus expressing the chemogenetic activator hM3Dq or an inactive mCherry control under the control of the CaMKIIα promoter into the infralimbic cortex (IL) of the mPFC (Fig. 1a, b). To confirm the efficacy of the chemogenetic stimulation, we measured the mRNA expression of neuronal activation and plasticity-related immediate early genes (IEGs) using qRT–PCR after the administration of Compound C21 (0.75 mg/kg), which is a specific activator of DREADDs[28]. Acute intraperitoneal injection two hours before tissue collection upregulated *cFos*, Homer1a and *NPAS4* expression but not *Arc* levels in the mPFC (Supplementary Fig. 1a). Prolonged stimulation using C21 (0.75mg/kg) administered via the drinking water overnight upregulated the expression of all the measured IEGs (Supplementary Fig. 1c, d). In contrast, acute C21 administration to control mice without the DREADD construct had no significant off-target effects on any of the investigated genes (Supplementary Fig. 1b).

To induce a depressive-like state, we utilized the chronic despair model (CDM), which involves subjecting animals to 10-min forced swim sessions daily for five consecutive days (Fig. 1a)[29]. This model yields a long-lasting depression-like phenotype, including increased immobility time in the classical forced swim test (FST) and tail suspension test (TST) and decreased sucrose preference (Fig. 1c, d and Supplementary Fig. 2a-c); moreover, this model is sensitive to both chronic monoaminergic antidepressants and acute ketamine treatment[16,30,31].

We used a multimodal approach to assess various aspects of depressive-like behavior. Two days after CDM induction, we administered C21 (0.75 mg/kg) via the drinking water overnight. To evaluate motivation and reward-oriented behavior, we conducted the nose-poke sucrose preference test (NP-SPT) in an IntelliCage[16,31,32] following a progressive ratio reinforcement schedule. Consistent with previous findings[16,31], the CDM resulted in significant anhedonia-like behavior, and this phenotype was reversed by overnight C21 treatment in mice expressing hM3Dq receptors in principal cells but not in mice expressing the mCherry control (Fig. 1c). Similarly, the CDM increased immobility time in both the FST (Fig. 1d) and TST (Supplementary Fig. 2a), and IL-specific DREADD activation restored the normal phenotype (Fig. 1d, e). Notably, neither exploratory activity in the IntelliCage (measured by corner visits) nor global locomotion in the open field test (OFT) was affected by CDM establishment (Fig. 1f and Supplementary Fig. 2c) or IL stimulation (Fig. 1f, g); these results excluded the possibility that DREADD stimulation induced hyperactivity. While not a direct feature of depression *per se*, anxious behavior is a common consequence of chronic stress. In the OFT, C21 treatment increased the time the hM3Dq-expressing mice spent in the center compared to control mice (Fig. 1h), indicating reduced anxiety-like behavior.

To assess exploratory behavior, we conducted a novel object exploration (NOE) test and measured the time the mice spent investigating previously unseen objects. IL activation significantly increased the time spent exploring both objects compared to control mice (Fig. 1i), indicating increased interest in novel stimuli. Social deficits represent a major component of depressive symptomatology and are both a consequence of and a risk factor for MDD[33,34]. Using the three-chamber task, we measured sociability as

the ratio of time spent exploring a novel social stimulus versus a novel object. IL stimulation significantly increased social preference in hM3Dq-expressing mice compared to mCherry control-expressing mice (Fig. 1j), suggesting enhanced sociability.

Additionally, to verify DREADD specificity, we compared hM3Dq-expressing mice that received either C21-supplemented water or regular drinking water as a control. Here, hM3Dq activation exerted antidepressant-like effects in the FST, TST, and NOE, although the effects in the social preference test did not reach significance (Supplementary Fig. 2d-e); these results confirmed that the antidepressant-like effects are specific to IL stimulation rather than unspecific effects of DREADD expression.

To establish the specificity of the role of IL in the antidepressant effect of mPFC stimulation, we conducted parallel DREADD experiments targeting the prelimbic cortex (PrL), which is another key mPFC subdivision that is located dorsal to the IL (Supplementary Fig. 2j). PrL activation did not affect immobility time or anhedonia-like behavior (Supplementary Fig. 2k-m), demonstrating that antidepressant-like effects specifically require IL, but not PrL activation.

IL stimulation rescues CDM-induced abolition of hippocampal synaptic plasticity

Chronic stress has been shown to disrupt hippocampal synaptic plasticity and this effect can be rescued by antidepressants such as ketamine or long-term fluoxetine treatment[27,35,36]. To investigate the effects of IL stimulation on hippocampal plasticity, we performed *ex vivo* recordings of CA1 pyramidal neurons in CDM mice. We induced associative LTP (aLTP) by pairing subthreshold excitatory postsynaptic potentials (EPSPs) evoked by Schaffer collateral stimulation with postsynaptic action potentials (125 EPSP→AP pairings at the theta-burst frequency; Fig. 2a, b). This resulted in a stable increase in EPSPs after 20–30 min in naive mice, whereas no such increase was observed in CDM mice, demonstrating a complete abolition of LTP (Fig. 2c, d). CDM-induced hippocampal aLTP blockade could be completely reversed by overnight IL activation (Fig. 2e, f) without affecting presynaptic function measured by the paired-pulse ratio (PPR, Supplementary Fig. 3a) or membrane properties (input resistance, Supplementary Fig. 3b), indicating a selective effect on associative plasticity. Overall, these results show that the IL stimulation reversed chronic-stress induced hippocampal aLTP deficits, demonstrating that PFC activity modulates hippocampal synaptic plasticity.

IL activation modulates hippocampal microcircuit dynamics

To investigate how IL stimulation affects HIP circuit dynamics, we used *in vivo* fiber photometry recordings in the ventral hippocampus (vHIP) of freely moving mice expressing hM3Dq receptors in IL principal cells and cell type-specific genetically encoded calcium indicators in the vHIP. We recorded both excitatory (CaMKIIα-GCaMP8m) and inhibitory (mDlx-jRGECO1a) vHIP neurons (Fig. 3a). We monitored Ca^{2+} signals in mice performing the TST 48 h after CDM induction and after overnight C21

treatment. Using a custom-trained DeepLabCut pose estimation model[37], we identified transitions between active (struggle) and passive (immobility) states.

Our analyses revealed increased peak amplitudes and areas under the curve (AUCs) during bouts of struggle after C21 treatment (Fig. 3b). Conversely, periods of immobility were associated with decreased Ca^{2+} activity, and IL stimulation resulted in increased negative deflection in both the peak amplitudes and AUCs (Fig. 3c). While inhibitory neuron responses increased during bouts of struggle, only difference in the AUC was significant (Fig. 3d, e). The global peak amplitudes during full periods of immobility or struggle remained unchanged after IL activation (Supplementary Fig. 4a, b).

These findings demonstrate that IL activation bidirectionally modulates HIP activity during behavioral transitions, increasing excitatory neuron responses during struggle and further suppressing these responses during immobility, with concurrent changes in inhibitory neuron dynamics. This increased state-dependent dynamics suggests that IL activation improves hippocampal “gain”, potentially contributing to its antidepressant effects.

Prefrontal IL stimulation induces hippocampal plasticity-related IEGs in a region-specific manner

The dorsal (dHIP) and the vHIP regions are functionally distinct, and are classically linked to cognition and emotion, respectively[38]. To assess whether IL stimulation differentially regulates these two compartments, we measured the mRNA expression of neuronal activation and plasticity-related IEGs in the dHIP and vHIP after CDM induction and IL DREADD activation (Fig. 4a). Acute intraperitoneal administration of C21 upregulated *cFos*, *Homer1a, NPAS4* and Arc in the ventral area but remained unchanged in the dorsal area (Fig. 4b, d). In contrast, acute C21 administration to control mice without the DREADD construct had no significant off-target effects on any of the investigated genes or hippocampal regions (Supplementary Fig. 5a, b). After a prolonged overnight stimulation, the expression of all the IEGs except *cFos* was increased in the vHIP; however, no changes were observed in the dHIP (Fig. 4c, e and Supplementary Fig. 5c, d).

These data suggest that IL stimulation increases neuronal activity and the expression of plasticity related genes specifically in the vHIP, identifying this hippocampal subregion as a key downstream target of IL activation.

IL stimulation increases ventral, but not dorsal hippocampal CA1 structural plasticity.

To assess the effects of IL stimulation on structural plasticity, which is another key feature that is altered in depression[7,14,17], we labeled input-specific presynaptic markers by immunohistochemistry (Fig. 4a, f). Then, we conducted three-dimensional quantification of synaptic density and volume in the CA1 region of both the ventral and dorsal HIP. We used three distinct markers: GAD65, which is a marker of inhibitory presynaptic boutons in the stratum lacunosum moleculare (SLM), and VGLUT1 and VGLUT2, which are

markers of excitatory presynaptic boutons in the stratum radiatum (SR) and SLM, respectively. These latter markers distinguish between intrinsic hippocampal or cortical inputs (VGLUT1) and subcortical/thalamic inputs (VGLUT2)[39,40]. After overnight IL stimulation, the GAD65 and VGLUT1 densities remained unchanged, but the VGLUT2 puncta density significantly increased in the vHIP but not in the dHIP SLM (Fig. 4g, h); suggesting a selective increase of subcortical inputs. In the mPFC, VGLUT2 and GAD65 density remained unchanged after overnight IL stimulation (Supplementary Fig. 5e, f). Finally, no change in the mean volume of VGLUT1, VGLUT2, or GAD65 puncta was observed in the dorsal or ventral HIP (Supplementary Fig. 5g-i).

Taken together, these results show that IL preferentially increases vHIP excitatory synapses from subcortical origins.

The RE gates IL-stimulation mediated antidepressant effects.

To investigate the circuit-related mechanisms mediating the effects of the IL on the HIP, we focused on the RE, which is a key relay structure that coordinates PFC–HIP communication[41,42]. Via a dual-chemogenetic approach, we simultaneously activated the IL while inhibiting the RE (Fig. 5a-c). After CDM induction, IL DREADD stimulation with the control construct in the RE (CaMKIIa-hM3Dq in the IL + CaMKIIa-mCherry in the RE) resulted in antidepressant-like effects in the FST (Fig. 5d). However, concurrent RE inhibition (CaMKIIa-hM3Dq in the IL + CaMKIIa-hM4Di in the RE) abolished these effects. RE inhibition alone had no effect on immobility time, indicating that the RE plays a specific role in mediating IL-driven effects (Fig. 5d). Additional behavioral tests revealed similar patterns: while mice expressing hM3Dq in the IL and mCherry in the RE spent increased time in the center during the OFT and increased time exploring the novel object, these effects were abolished by RE inhibition (Fig. 5e, f).

To determine whether the RE also mediates the effects of the IL on associative plasticity in the HIP, we analyzed patch–clamp recordings of *ex vivo* HIP slices from CDM mice expressing the same viral constructs. Following our established protocol, we induced aLTP via paired Schaffer collateral-postsynaptic stimulation. While IL stimulation (CaMKIIa-hM3Dq) with the control virus in the RE (CaMKIIa-mCherry) successfully restored aLTP, which is consistent with our results above, concurrent RE inhibition (CaMKIIa-hM4Di) prevented this restoration, maintaining the CDM-associated plasticity deficit (Fig. 5g, h, Supplementary Fig. 6a, b).

These results determine the RE as an essential mediator of both the behavioral and plasticity-related effects of IL activation, revealing the critical role of the IL→RE→HIP circuit in antidepressant response (Fig. 5i).

The RE is required for ketamine antidepressant effect and plasticity restoration.

To investigate the broader role of the RE in the antidepressant response, we examined its role in the therapeutic effect of ketamine. We used two approaches to inhibit RE function (Fig. 6a): direct local RE inactivation using inhibitory DREADDs (CaMKIIa-hM4Di) and selective inhibition of IL→RE projections

using an intersectional strategy that combines retrograde AAV-Cre in the RE and Cre-dependent hM4Di in the IL (Fig. 6b-d). Consistent with previous findings[16,31], ketamine (10 mg/kg) reversed CDM-induced immobility in control non-AAV-injected mice (Supplementary Fig. 6a). However, both global RE inhibition (CaMKIIa-hM4Di in RE) and selective IL→RE projection inhibition (CaMKIIa-DIO-hM4Di in mPFC + retro-hSyn-CRE in RE) completely blocked this antidepressant response (Fig. 6e). Similarly, while ketamine restored hippocampal aLTP in control mice (Supplementary Fig. 7b, c); IL→RE projection inhibition selectively prevented this restoration (Fig. 6f, g and Supplementary Fig. 7d, e), despite the well described local effects of ketamine on hippocampal circuits[27].

These findings demonstrate that the RE is essential not only for IL stimulation-induced effects but also for the antidepressant and neuroplastic effect of ketamine (Fig. 6h), suggesting that the IL→RE→HIP circuit represents a critical pathway in the treatment of depression (Fig. 7).

Methods

Animals and Husbandry

Wild-type C57Bl6J (RRID: IMSR_JAX:000664) mice were obtained from Charles River (France and Germany) and maintained at the animal husbandry facilities of the Universities of Freiburg (Center for Experimental Models and Transgenic Service) and Strasbourg (Chrnobiotron). The Chronobiotron facility is registered for animal experimentation (Agreement A67-2018-38). All the procedures were performed in accordance with the German animal protection law (TierSchG), FELASA (http://www.felasa.eu), the guide for the care and use of laboratory animals of the national animal welfare body GV-SOLAS (http://www.gv-solas.de) and the EU Directive 2010/63/EU for animal experiments. Moreover, the procedures were approved by animal review boards in Germany (Regierungspräsidium Freiburg, licenses G-19/44 and G24/033) or France (CREMEAS, APAFIS n°2020042818477700), and all the animal care protocols followed national and international standards, with consistent documentation of procedures. Power calculations were conducted before experiments to assess animal behavior to minimize the number of animals used. Both male and female mice were included throughout the study. All the mice were at least 8 weeks old at the start of experimental procedures and were housed in a temperature- and humidity-controlled environment, with ad libitum access to food and water, under a 12-h light-dark cycle.

Surgical procedures

Before surgery, the mice received subcutaneous injections of carprofen (4 mg/kg) and buprenorphine (0.1 mg/kg). Mice were anesthetized with isoflurane (4% for induction, 1.5% for maintenance) and positioned in a stereotaxic frame (51730UD, Stoelting, USA). Ophthalmic gel (Ocrygel, TVM, UK) was applied to prevent corneal drying, and body temperature was maintained using a heated pad. A total of 300 nL of viral suspension, namely, a suspension of ssAAV-5/2-mCaMKIIa-hM3D(Gq)_mCherry-WPRE-hGHp(A) (v96-5, Viral Vector Facility VVF, Switzerland), ssAAV-5/2-mCaMKIIa-mCherry-WPRE-hGHp(A)

(v199-5, VVF, Switzerland), AAV5-hSyn-DIO-mCherry (v116-5, VVF, Switzerland) or AAV5-hsyn-DIO-hm3d(Gq)-mCherry (44361-AAV5, Addgene, USA), was bilaterally injected into the IL (+ 1.7 mm AP, +/-3 ML, -2.8 DV relative to Bregma) or PL (+ 1.7 AP, +/-3 ML, -2.4 DV) regions of the PFC of WT mice using a 30G syringe (Hamilton Neuros syringe) and a microinjection syringe pump (UMP3T, WPI, USA) at a rate of 200 nL/min. For the RE injections, a similar process was followed to unilaterally inject ssAAV-5/2-mCaMKIIa-hM4d(Gi)_mCherry-WPRE-hGHp(A) (v102-5, VVF, Switzerland), ssAAV-5/2-mCaMKIIa-mCherry-WPRE-hGHp(A) (v199-5, VVF, Switzerland), or AAV(retro).hSyn.HI.eGFP-CRE.WPRESV40 (105540-AAVrg, Addgene, USA) at a 15° angle (+ 1.7 AP, -1.1ML, -4.5DV). After injection, the syringe was held in place for five minutes before being slowly withdrawn. pAAV-hSyn-DIO-hM3D(Gq)-mCherry was a gift from Bryan Roth, pENN.AAV.hSyn.HI.eGFP-Cre.WPRE.SV40 was a gift from James M. Wilson.

For fiber photometry, a genetically encoded calcium indicator (GeCI) was unilaterally injected in the vHIP, and the left and right side were randomized. For inhibitory neurons, AAV5-mDlx-HBB-chl-NES_jRGECO1a-WPRE-SV40a (v527-5, VVF, Switzerland) was injected to record inhibitory neurons (-3.4 AP, -3 ML, -4 DV) and AAV5-mCaMKIIa-jGCaMP8m-WPRE-bGHp (v630-5, VVF, Switzerland) was injected to record excitatory neurons (AP = -3.4 AP, -3.4 ML, -4 DV). The mice were subsequently implanted with a ferrule-coupled optical fiber (400 µm core diameter, 0.37 NA, MFC_400/470 – 0.37_4.5 mm_MF2.5_FLT, Doric Lenses, Canada) above the injection site. The implant was stabilized with three screws around it and secured with dental cement (Light Curing Nano Flowable Composite, Dline, Lithuania), which was solidified using a UV-light-emitting device. The mice received 0.1 mg/kg buprenorphine 6 h postsurgery and carprofen (4 mg/kg, s.c.) every 12 h for 3 days. The mice were allowed to recover for 3 weeks before experimental procedures.

Behavioral Procedures

Chronic despair model (CDM): The CDM model is an established mouse model of depression-like behavior and reliably predicts the effects of antidepressants[29–31,84]. To establish this model, mice were forced to swim in a glass cylinder (Ø 26 cm, 60 cm high) filled with water (21–23°C) to a depth of 25 cm for 10 min on 5 consecutive days (induction phase). The immobility time was measured in each session. After swimming, the animals were gently dried and kept in a cage under a heating lamp for an additional ten minutes. Then, the mice were allowed to rest for two days in their home cages before the readout experiment was performed on the third day after the induction phase.

DREADD activation: C21 (#5548, Tocris, United Kingdom) was dissolved in the drinking water of the mice, and this water was given to the mice overnight (6p.m to 8a.m). The dose was calculated considering an average consumption of 5 mL per mouse per night.

Forced swim test (FST): For the classical FST, mice were placed in a transparent glass cylinder (15 cm diameter) filled to a height of 20 cm with water (22–25°C). Immobility time was assessed during a swim session. Mice were considered immobile when they floated in an upright position and made only minimal movements to keep their head above the water.

Open field test (OFT): The test was performed in a square arena (50 x 50 cm) with a virtual square area of 30 x 30 cm in the center. The open field was surrounded by a 35-cm high wall made of gray PVC. The mice were placed in the center of the field and allowed to move freely. Behavior was recorded for 10 min, and total distance traveled and time spent in the center area were analyzed.

Tail suspension task: For the TST, mice were attached via their tails (1–1.5 cm from the tip of the tail) to a horizontal bar located 40 cm above a table. Each trial was conducted for 6 min, and immobility time was determined.

Novel object exploration: Mice were allowed to explore an open field (50x50 cm) for 10 min. Then, two objects (maximum size of 10x10x10 cm) were added two out edges of the space. Behavior was recorded for 10 min, and then, the video was stopped and the mouse was returned to its cage. Post hoc analysis of the explorations was performed using Ethovision XT (Noldus, Netherlands).

Three chamber task (3ChT): A 3-chamber apparatus (60x25x23 cm, chambers of 20x25x23 cm) was used to record the sociability of the mice. The mice were able to explore the full apparatus for 10 min. Then, the external rooms were closed, and the mouses were restricted in the central room. An object and a mouse that was restricted to a meshed cup were placed in the outer rooms. Then, the doors were opened, and interactions were recorded for 10 min. Interactions of the test mouse with the object or the social visitor were quantified using the Ethovision XT (Noldus, Netherlands) software.

Nosepoke sucrose preference test (nSPT): The IntelliCage system (TSE Systems, Germany), which allows automatic analysis of spontaneous and exploratory behavior and drinking preference of rodents, was used. Radiofrequency identification transponders were implanted in the mice. IntelliCage comprises a common space in the middle and four corners were measurements are recorded. Up to 16 group-housed mice can be given free access to food in the center, and water is supplied in the corners (two zipper bottles each) behind electronically managed doors. The corners can be visited by only one mouse at a time. Using IntelliCage Plus software (TSE Systems, Germany), the system records i) the number and duration of visits to the corners, ii) the number of times a mouse pokes a door with its nose (approaches), and iii) the number of times a mouse licked a drinking bottle. Initially, the mice were allowed to adapt to the IntelliCage for five days and provided free access to food and water in all the corners. Then, for three days, the animals were habituated to sucrose (each corner had one bottle that contained 1% sucrose solution and one bottle that contained water; the right/left position of all the bottles were exchanged every day) and subjected to the nosepoke protocol. The mice had to poke a door with their nose to open it and had access both water and sucrose solution. Next, an nSPT paradigm[16,31] in which gradually increasing effort (number of times a mouse had to poke a door with its nose to open the door) was needed to access the bottles containing sucrose solution for a short period (24 h), was used to measure sucrose preference. In this protocol, each door was opened in response to a nosepoke and closed after the mouse drank from the sucrose solution-containing bottle for 5 s, but the mice were allowed to consume plain water for an unlimited amount of time. The number of nosepokes needed to access the bottle containing sucrose solution progressively increased (1, 2, 3, 4, 5, 6, and 7) after each of

the 10 drinking sessions. This test was used to assess the drive to obtain a reward; a decreased sucrose preference indicated reduced reward behavior. For every side, the number of times a mouse licked a bottle was counted, and the mean sucrose preference was calculated as the percentage of times a mouse licked a bottle containing sucrose solution relative to the total number of times a mouse licked any bottle.

Quantitative real-time PCR (qRT–PCR)

The mice were killed by cervical dislocation, and their brains were rapidly extracted and coronally sectioned. The regions of interest were microdissected, quickly frozen on dry ice and stored at -80°C until RNA was isolated. The RNA extraction and expression analyses were performed as previously described[16]. Briefly, the tissues were homogenized in guanidine thiocyanate/2-mercaptoethanol buffer, and total RNA was extracted using the sodium acetate/phenol/chloroform/isoamyl alcohol method. Then, the samples were precipitated with isopropanol and washed twice with 70% ethanol. The resulting pellets were dissolved in RNase-free Tris-HCl buffer (pH 7.0), and the RNA concentrations were measured using a spectrophotometer (BioPhotometer; Eppendorf). Reverse transcription was performed with 1 mg of total RNA using M-MLV reverse transcriptase (Promega). Quantitative real-time PCR was performed on a 7300 Real-Time PCR System with Sequence Detection Software qPCR v1.3.1 (Applied Biosystems) utilizing Fast SYBR™ Green Master Mix (4385612, Applied Biosystems). All the qRT–PCR experiments were performed in a blinded manner, as the coded cDNA samples were pipetted by a technician. The target gene mRNA levels were normalized to the levels of apolipoprotein E (*ApoE*), glyceraldehyde-3-phosphate dehydrogenase (*GAPDH*) and *s12* RNA. The sequences of the primers that were used were as follows: *ApoE*: 5‘-CCTGAACCGCTTCTGGGATT-3‘, 5‘-GCTCTTCCTGGACCTGGTCA-3‘; *GAPDH*: 5‘-TGTCCGTCGTGGATCTGAC-3‘, 5‘-CCTGCTTCACCACCTTCTTG-3‘; *s12*: 5‘-GCCCTCATCCACGATGGCCT-3‘, 5‘-ACAGATGGGCTTGGCGCTTGT-3‘; Homer1a: 5‘-CAAACACTGTTTATGGACTG-3‘, 5‘-TGCTGAATTGAATGTGTACC-3‘; Arc: 5 $-TGG\mathbb{C}\mathbb{C}CAGCAGTGA\top CATAC-3$’, 5-TGCCCTTTCCAGACATGGCAGC-3’; c-fos: 5'-ATCCTTGGAGCCAGTCAAGA-3', 5'-ATGATGCCGGAAACAAGAAG-3'; *Npas4*: 5'-CAGGGACAGGTTAGGGTTCA-3', 5'-TTCAGCAGATCAGCCAGTTG-3'

Electrophysiology

The mice were preoxygenated in a 100% oxygen atmosphere for 5 min before cervical dislocation and then decapitated according to national and institutional guidelines. Three hundred-micrometer-thick transverse slices from the HIP were cut with a vibratome (VT1200, Leica Biosystems, Germany). The slices were prepared in artificial cerebrospinal fluid (aCSF) containing (in mM): 125 NaCl, 25 $NaHCO_3$, 1.25 NaH_2PO_4, 2.5 KCl, 1 $MgCl_2$, 27 glucose, and 2 $CaCl_2$ (bubbled with carbogen (95% O_2, 5% CO_2)).

After incubation for 20 min at 35°C, the slices were maintained at room temperature in aCSF, transferred to the recording chamber (volume of approx. 2–3 ml) and continuously superfused with aCSF (rate of approx. 5–10 ml/min-1). Differential interference contrast video microscopy was used to assess the location and morphology of CA1 pyramidal neurons (Zeiss Axioskop 2 FS plus, Zeiss Microscopy, Germany). In addition to optical identification, neurons are classified according to the adaptation of their characteristic firing frequency to long depolarizing current pulses. Borosilicate glass tubes (2.0 mm outer diameter, 0.5 mm wall thickness; Hilgenberg, Germany) were used to pull the patch pipettes. The pipettes had an open resistance of 5–10 MΩ, and the series resistance (Rs) of 10–50 MΩ was compensated by a bridge balance. The patch pipettes were filled with two different internal solutions for current clamp (EPSP) and voltage clamp (current) measurements. The internal solution for the current clamp contained (in mM) 132 K-gluconate, 20 KCl, 2 $MgCl_2$, 10 HEPES, 0.1 EGTA, 4 Na_2ATP, and 0.3 NaGTP (pH adjusted to 7.2 with KOH). The internal solution for voltage clamp measurements contained 135 Cs-gluconate, 2 CsCl, 5 QX314, 10 HEPES, 10 EGTA, 2 $MgCl_2$, 2 Na2ATP, and 2 TEA-Cl (pH adjusted to 7.2 with HCl). Osmolarity (280–300 mosmol/L) was controlled at the beginning of each experimental day with an osmometer (Osmomat, Gonotec, Germany).

A stimulation pipette (a patch pipette with an open resistance of 1–3 MΩ when filled with internal solution) was placed superficially in the stratum radiatum of the CA1 region approximately 30–50 μm from the PC layer. Subthreshold EPSPs of 2–7 mV were evoked by Schaffer collateral stimulation with voltage pulses of 10–80 V (frequency of 0.1 Hz, duration of 200 μs) using a stimulus isolator (Model 2100 isolated pulse stimulator, A-M Systems, USA). The resting membrane potentials were between − 75 and − 65 mV, and the holding potential was − 70 mV. Hyperpolarizing voltage test pulses (50 ms/-5 mV) were applied to assess the input (Rm) and series (Rs) resistance after every 10th EPSP. EPSPs were combined with postsynaptic action potentials (APs) triggered by short (3 ms) 700 pA current injections via the patch-clamp electrode. Five EPSPs and five postsynaptic APs were paired at 100 Hz with a 5 ms delay (AP after EPSP). Five of these bursts of synchronized EPSP→AP pairs were applied at the theta frequency (5 Hz), followed by an interval of 10 s and 4 more theta blocks, resulting in 125 EPSP/AP pairings.

EPC-10 amplifiers (HEKA, Germany) were used, and the signals were filtered at 5 kHz. Patchmaster NEXT software (Version 1.2, HEKA, Germany) was used for data acquisition and initial analysis. All the experiments were performed at room temperature.

The experiments were discarded if (i) the Rs changed by more than 30% during the experiment, (ii) evidence of ictal discharges was observed, (iii) the membrane potential between the start and end of the experiment differed by more than 5 mV, or (iv) the neurons did not respond to a firing pattern control pulse at the beginning and end of the experiments. A maximum of two hippocampal slices per animal were used. All the groups included at least 6 animals.

Analysis of LTP: In the LTP figures, each dot represents six consecutive averaged maximum EPSP amplitudes ± SEM. The horizontal bars at 25–30 min indicate significant differences between the

baseline and postinduction EPSP amplitudes within each experimental group. The mean amplitude of 30 consecutive EPSPs was calculated before the induction protocol to determine the baseline amplitude. Twenty-five minutes after LTP induction, the mean amplitude of 30 consecutive EPSPs was calculated and compared to the baseline value from the same experiment with a two-tailed t test. Changes in EPSP amplitudes are expressed as percentages of the baseline measurements and were analyzed for each experimental group to quantify the degree of LTP.

Immunohistochemistry

After intracardiac perfusion, the brains of the mice were extracted with 20 mL of ice-cold phosphate-buffered saline (PBS; 8.1 mM Na_2HPO_4, 138 mM NaCl, 2.7 mM KCl and 1.47 mM KH_2PO_4 [pH 7.4]), followed by 15 mL of 4% paraformaldehyde (PFA) in PBS. The brains were subsequently fixed in 4% PFA/PBS for 6 hours at 4°C and then cryoprotected for 48 hours in a 30% sucrose/PBS solution at 4°C. After being sectioned with a cryostat, 30-µm-thick sections were washed and blocked with 4% normal goat serum in PBS for 1 h at room temperature. The primary antibodies were diluted in PBS, 0.3% Triton X-100, and 1% goat serum, added to the sections, and incubated overnight at 4°C with agitation. The sections were then washed three times for five minutes each with PBS supplemented with 1% Triton X-100, followed by incubation for one hour at room temperature with secondary antibodies diluted in PBS supplemented with 1% Triton X-100 and 1% goat serum. The sections were then incubated for 15 min at room temperature with the nuclear stain 4,6-diamidino-2-phenylindole (DAPI; Thermo Fisher Scientific, USA; 1:1000) in PBS supplemented with 0.2% Triton. After washing, the sections were mounted with Mowiol-DABCO (803456, Merck, Germany).

The following primary antibodies were used: guinea pig polyclonal anti-VGLUT1 (AB5905, 1:1000; Millipore, USA, lot #4141952), anti-VGLUT2 (AB2251-I, 1:1000; Millipore, USA, lot # 4137617) and mouse anti-GAD65 (ab26113, 1:500; Abcam, United Kingdom, lot #GR3308495-2). The following secondary antibodies were used: goat polyclonal anti-guinea pig Alexa Fluor 594 (Invitrogen, USA; A-11076, 2 µg/mL; lot #2540867) and goat polyclonal anti-mouse Alexa Fluor 488 (A-32723, 2 µg/mL; Invitrogen, USA; lot #XA336883). All the images were captured using a Zeiss Celldiscoverer 7 microscope equipped with a confocal LSM 900 with AiryScan 2. The objective used was a Plan-Apochromat 50 ×/1.2 W, N.A. 1.2, H_2O immersion. The laser intensity and gain were set to occupy the full dynamic range of the detector.

Morphological analysis

All the presynaptic quantifications were performed by a blinded experimenter. Images were analyzed using the supervised machine learning software Ilastik[85]: pixel classification and object detection workflow.

Fiber photometry: Data acquisition and analysis

The fiber photometry setup consisted of a Doric fiber photometry console (FPC, Doric Lenses, Canada), a 6-port fluorescent minicube with an integrated LED and detector (iIFMC6-G2, Doric Lenses, Canada), and a USB DAQ board (USB-6210, National Instruments, USA). The minicube was connected to the implanted ferrule via a low-autofluorescence patch cord (400 µm core diameter, 0.37 NA, MFP_400/440/1100 – 0.37_5m_FCM-MF2.5_LAF, Doric Lenses, Canada) and interconnection sleeve (SLEEVE_BR_2.5-BK, Doric, Canada). Excitation light was delivered from LEDs at 470 nm (for the GCaMP signal) or 520 nm (for RGECO1a). An isosbestic channel (405 nm LED) was used for both the green and red sensors to control for motion artifacts and photobleaching. The emission light was collected through the same optical fiber, passed through a GFP emission filter (525/50 nm) for the GCaMP signals or an RFP emission filter (630/60 nm) for the RGECO1a signals, and reached the built-in photodetector set up in lock-in detection mode. Videos of the mice were simultaneously recorded with the IR-illuminated camera at a 30 Hz frame rate (DMK DMK 33GX290, Imaging Source). The data were collected by the DAQ at a 2-kHz sampling rate using a custom LabVIEW script (National Instruments, USA).

Fiber photometry data were first demodulated using a custom MATLAB script, resulting in an effective 20-Hz rate for fluorescent recordings. The signal analysis pipeline was then implemented following a custom adaptation of the GuPPy python toolbox[86]. Briefly, the signal was first filtered using a zero-phase moving average linear digital filter, an isosbestic control was fitted to the signal (least square linear regression), and ΔF/F was calculated by subtracting and dividing the control data from the signal data. Mouse behavior was recorded during a session and automatically analyzed using DeepLabCut[37] for pose estimation. Episodes of immobility and struggle were filtered using two temporal criteria: each bout was required to last a minimum duration of 3 s and had to be preceded by at least 3 s of the opposite behavior. The resulting timestamps were analyzed together with the ΔF/F signal using a custom python script. To calculate the global peak amplitude, transients were detected in the full dff periods of struggle or immobility using the find_peaks library of scipy.

Statistical analysis

All values are presented as the means, and the error bars represent the SEMs in the figures. For the statistical analyses, GraphPad Prism version 10.0 (GraphPad Software, USA) was used. To test for significance within experimental groups, we used a two-tailed paired Student’s t test or a Wilcoxon signed rank test. To compare two experimental groups, either an unpaired Student’s t test or the Mann–Whitney test was performed. Welch's correction was applied to t tests when variances were significantly different. To analyze differences among several treatment groups, one or two-way analysis of variance (ANOVA) followed by Bonferroni’s or Tukey’s post hoc tests was used. The outliers were systematically excluded using ROUT methods set to 1%. All the statistical tests were two-tailed if applicable. Significance levels are indicated by asterisks in the figures: *$p < 0.05$, **$p < 0.01$, ***$p < 0.001$. The exact p and F values as well as the tests that were used to analyze each group are listed in Source Data files.

Statistical analysis summaries are mentioned in the figure legends. For all the molecular and behavioral studies, the mice were randomly assigned to groups. Most behavioral and molecular results were confirmed via independent replication of the experiments, as shown in Source Data files. Additionally, the investigators were blinded to the treatment groups until the data were collected. Sample sizes were determined on the basis of extensive laboratory experience[16,27,30,31] and were verified via power analysis.

Discussion

Depression is a complex disorder that is characterized by a wide range of symptoms and the involvement of multiple, likely overlapping, biological processes, including molecular, circuit-related, and electrophysiological mechanisms. Despite this heterogeneity, studies on diverse patient cohorts and animal models have highlighted a significant degree of convergence in several pathophysiological features. Among these features, deficits in neuroplasticity—including associative plasticity deficits and excitatory synapse downregulation in the PFC and HIP—have emerged as consistent findings across clinical and preclinical studies. These synaptic deficits are accompanied by structural changes, such as dendritic spine loss and altered synaptic density, and these changes can be targeted by treatment with fast-acting antidepressants[7,17,43,44]. Another key feature that has been consistently reported across studies involves changes in specific brain circuits, and robust evidence has indicated that PFC and HIP abnormalities are major factors that contribute to the pathophysiology of depression[21,45].

In this study, we identified a circuit that connects these two pivotal brain regions via the RE of the thalamus. This circuit not only drives antidepressant effects but also controls hippocampal neuroplasticity and microcircuit dynamics. Notably, activation of the IL alone was sufficient to induce antidepressant-like effects in several behavioral domains. This circuit specificity is highlighted by our finding that PrL stimulation did not elicit antidepressant-like effects, which is consistent with previous results showing opposing roles of the IL and PrL in emotional regulation[46].

Our results demonstrate that the effects of IL stimulation extended to the HIP, which is another structure that is highly impacted in depression. HIP atrophy[10,47,48], decreased cell size[49], reduced CA1 volume[50] and synaptic loss have been associated with different stages of the disease. IL stimulation induced region-specific molecular changes in the HIP, leading to the upregulation of IEGs such as *cFos*, *Homer1a*, and *NPAS4* in the ventral but not the dorsal HIP. They act as markers of neuronal activation and synaptic plasticity, and their upregulation indicated that IL stimulation increased neuronal activity in these regions. Indeed, c-Fos is a transcription factor that directly influences synaptic plasticity and has been associated with mood disorders[51]. Notably, Homer1a regulates glutamate receptor function and intracellular calcium signaling, and its expression is affected by stress and antidepressants[16,30]. NPAS4 balances excitatory and inhibitory synapses, which is crucial for emotional stability, and its dysregulation is associated with depressive-like behaviors[52]; Arc modulates synaptic strength by directly regulating

AMPA receptor trafficking, and its dysfunction has been associated with cognitive deficits and mood disorders[53].

To investigate circuit-specific synaptic changes, we studied input-specific presynaptic markers. VGLUT1 and VGLUT2 show complementary distribution patterns in the brain, with VGLUT1 being predominantly expressed in cortical regions and intrinsic hippocampal circuits and whereas VGLUT2 being expressed mainly in subcortical projections, including those from the supramammillary area and the RE[39,40,54]. The distribution of VGLUT2 is consistent with its presence mainly in the SLM of the CA1 region, which is a major zone of thalamic termination[55,56]. Here, the specific increase in VGLUT2 expression in the ventral CA1 and IL regions suggested an increase in connections arising from a thalamic (likely RE) origin, although this link remains unproven. This regional specificity is functionally relevant, as the vHIP has been implicated in emotional processing and stress responses, whereas the dHIP is more involved in spatial cognition and memory[38]. Furthermore, the anatomical pathway that links the mPFC to the HIP through the RE preferentially targets the intermediate and vHIP[55,57], and the vHIP projects back to the mPFC[58], suggesting the presence of a functional loop (Fig. 7).

Our results directly link circuit-level analysis with neuroplasticity, which is another key mechanism that has been implicated in responses to antidepressants[7,26]. We provide compelling evidence that chronic stress-induced impairments in hippocampal LTP can be fully reversed by stimulation of the IL. This restoration of plasticity reproduces the effects of ketamine or long-term selective serotonin reuptake inhibitor (SSRI) treatment[27,59], which is considered a crucial criterion for antidepressant response[60].

Additionally, we used *in vivo* fiber photometry to directly monitor vHIP activity during TST, and we found that IL stimulation bidirectionally increased the dynamic range of vHIP responses between active and passive coping behavioral states. A recent theoretical framework proposes that the vHIP is a hub that links external stimuli to internal emotional and motivational drives[61]. The vHIP has been shown to encode the anxiogenic features of an environment to enable appropriate defensive responses[62], and it is implicated in social encoding[63] and susceptibility to stress and depression[64]. Furthermore, increased excitability and activity-dependent processes in the dentate gyrus have been associated with antidepressant-like effects[45]. Concurrent with increased HIP plasticity, our findings suggest that IL stimulation increases HIP processing and could participate in the modulation of emotional processing during antidepressant therapy.

The RE is a key node that synchronizes mPFC-HIP activity[65], supporting the flow of information between these structures. Functionally, the RE plays a crucial role in aversive memory specificity and extinction. RE inhibition leads to persistent memories of fear after stimulus removal[66] and maladaptive generalization of fear to unrelated stimuli[67]. Despite its established roles in memory processing, the involvement of the RE in the response to antidepressants remains largely unexplored. While one study reported that RE lesions exert antidepressant-like effects[68], the use of the FST in two sessions in that study—which cannot exclude the involvement of learning processes—raises a critical concern about the

interpretation of the results. One plausible hypothesis is that RE inhibition could disrupt the processing of aversive memories caused by the FST; thus, these results could be interpreted as resilience rather than an antidepressant effect. Further studies are needed to elucidate the role of the RE in resilience and the establishment of a depressive-like phenotype.

Our results following RE inhibition strongly suggest that the antidepressant effects of IL stimulation and the restoration of HIP plasticity are mediated by the IL->RE->HIP pathway. The RE targets the HIP at the SLM of the CA1 region, which coincides with our observation of increased VGLUT2 synaptic density and suggests that IL stimulation-induced structural plasticity is conveyed, at least in part, through increased RE synapses. The RE targets both excitatory and inhibitory neurons in the HIP; however, the precise nature of its inhibitory targets (Oriens-lacunosum-molecular, Calretinin, or Neurogliaform cells) is yet to be fully understood[56,69]

We found that inhibition of either the RE or IL->RE projections abolishes both the antidepressant effects of ketamine and the restoration of hippocampal LTP. This finding is striking, given that the effect of ketamine on LTP is mediated (at least in part) through its direct effects on the HIP, particularly through the disinhibition of pyramidal neurons[27,59,70]. One possibility is that while ketamine acts acutely to restore hippocampal LTP through local mechanisms, the maintenance of this effect requires the sustained engagement of a broader IL → RE → HIP → mPFC loop. Indeed, this ascending pathway projects back to the PFC, forming a loop that is important for hippocampal–prefrontal synchrony, which is important for memory and emotional processing[71]. Alternatively, ketamine could act at multiple points and/or particularly on mPFC, to activate this loop, and this activation might be necessary to exert antidepressant effects and restore plasticity in the HIP. Inhibition of any element of this chain would prevent the activation of the loop and therefore disrupt the effect, abolishing both the antidepressant effects and neuroplastic benefits of mPFC stimulation or ketamine. This circuit-based interpretation is supported by previous work that showed that activation of vHIP → mPFC projections not only reproduces but also is necessary for the antidepressant effects of ketamine[72] and that vHIP inputs preferentially target RE-projecting IL neurons[73], thereby closing this loop driving antidepressant response and controlling hippocampal plasticity.

This circuit may not be the only network underlying depression. For instance, another circuit that is hypothesized to mediate the antidepressant effects of ketamine is the lateral habenula (LHb), which is the "antireward center" of the brain[74,75]. The LHb is a highly connected hub structure that integrates inputs from diverse brain regions, including direct projections from the mPFC[76]. Thereby, such circuit mechanisms involving the LHb and the IL → RE → HIP circuit could theoretically operate inline, or on the contrary constitute independent and parallel mechanisms. Furthermore, MDD affects limbic structures that are important for motivational, social, and anhedonia-like behaviors, such as the NAc, the vHIP and the VTA[77,78]. The IL → RE → vHIP circuit is strongly connected to these structures, and the mPFC plays a putative role in the top-down control of these structures[64,79]. Given that IL stimulation affects motivational, social, and anhedonia-like behaviors, which are highly dependent on limbic structures, our

findings suggest that stimulation of this circuit might be a central "starting point" for antidepressant effects, potentially spreading to multiple downstream targets.

Recent theories posit that neuroplasticity provides neural networks with the ability to adapt to intrinsic and extrinsic stimuli[26,80]. While the initial suppression of plasticity under stress conditions might be a protective mechanism that reestablishes homeostatic balance and prevents excessive impacts of a repeatedly negative environment[81], prolonged plasticity disruption can become maladaptive and contribute to psychiatric disorders such as depression[44]. LTP measurements in hippocampal slices provide a rather “binary” readout of associative plasticity: present in healthy condition, it is abolished in a pathological state and restored after antidepressant treatment. Our manipulations of the IL → RE → HIP circuit reflect this binary nature, as activating this circuit “turns on” hippocampal LTP while disrupting it prevents this effect, maintaining LTP in an “off” state. Therefore, we hypothesize that this circuit might provide a pathway to alleviate the maladaptive inhibition of LTP that is observed in depression, analogous to resetting a safety switch.

Altogether, our study unifies two prominent theoretical frameworks for understanding depression pathophysiology, namely, the circuitry hypothesis and the neuroplasticity hypothesis. We identified the IL → RE → vHIP circuit as a central and converging network that regulates the response to antidepressant therapy and plasticity in the hippocampus. Targeted stimulation of this circuit might facilitate potent antidepressant benefits while avoiding off-target effects on undesirable circuits, which is a plausible cause of the adverse effects of pharmacotherapies.

Recent developments in brain stimulation techniques, such as DBS, TMS and transcranial focus ultrasound stimulation (tFUS), have provided unique opportunities for the targeted treatment of neuropsychiatric disorders[9,18,82,83]; however, the effectiveness of these approaches is currently limited by an incomplete understanding of the brain circuits involved. Further studies of the IL → RE → vHIP network could contribute to addressing the urgent need for novel strategies for the treatment of depression.

Declarations

Reporting summary

Further information on the research design is available in the Nature Research Reporting Summary linked to this article.

Data availability

The datasets generated and/or analyzed during the current study can be found in the paper and the supplementary materials. Source data are provided with this paper.

Code availability

Custom Python script used for analyzing fiber photometry data in Figure 3 is available in our GitHub repository (https://github.com/mveleanu/veleanu_et_al). Research materials will be made available by the corresponding author on a reasonable request.

Acknowledgements

The authors thank Dr. James M. Wilson and Dr. Bryan Roth for distributing the AAV(retro).hSyn.HI.eGFP-CRE.WPRESV40 and AAV5-hsyn-DIO-hm3d(Gq)-mCherry viruses. We thank the staff of the Life Imaging Center (LIC) of the Albert-Ludwigs University Freiburg for help with their microscopy resources, and the excellent support in image recording and analysis. The study was funded by grants from the German Research Council (SE 2666/2-1 and SE 2666/2-3) to T.S and C.N., and NO370/7-1 (C.N.), Medical Research Foundation (FRM) (AJE201912009450), University of Strasbourg Institute for Advanced Study (USIAS) (2020-035) to T.S., University of Strasbourg ITI NeuroStra (as part of the ITI 2021-2028 program of the University of Strasbourg, CNRS and Inserm, supported by IdEx Unistra ANR-10-IDEX-0002 under the framework of the French Program *Investments for the Future*) to T.S, the Hans. A. Krebs Medical Scientist Fellowship Program to M.V., and Berta-Ottenstein-Program for Clinician Scientists, Faculty of Medicine, University of Freiburg, Germany to S.V.

Author contributions

Conceptualization: M.V., T.S. and S.V., methodology: M.V., T.S. and S.V., investigation: M.V., J.W., T.S., L.S., D.S., M.A., L.R., G.S.M., S.Z., Z.B., A.B., M.B., A.C. and S.A.D., resources: T.S., C.N. and K.D., writing – original draft: M.V., writing – review and editing: M.V., T.S., L.S., T.C., S.V. and C.N, supervision: T.S. and S.V., funding acquisition: T.S., M.V. and C.N.

Competing interests

C.N. and K.D. received lecture fees and advisory board honoraria from Johnson & Johnson, the manufacturer of Esketamine. C.N. received research support as a principal investigator in clinical trials sponsored by Johnson & Johnson. C.N. received honoraria as a member of a DMC board by Novartis. T.S. received honoraria consulting Primetime Life Sciences, LLC. All other authors declare that they have no competing interests.

References

1. Depressive disorder (depression). https://www.who.int/news-room/fact-sheets/detail/depression
2. Gill K et al (2025) Examining the needs, outcomes and current treatment pathways of 2461 people with treatment-resistant depression: mixed-methods study. Br J Psychiatry 1–8. 10.1192/bjp.2024.275

3. Krystal JH, Abdallah CG, Sanacora G, Charney DS, Duman RS (2019) Ketamine: A Paradigm Shift for Depression Research and Treatment. Neuron 101:774–778
4. Castrén E (2005) Is mood chemistry? Nat Rev Neurosci 6:241–246
5. Spellman T, Liston C (2020) Toward Circuit Mechanisms of Pathophysiology in Depression. Am J Psychiatry 177:381–390
6. Page CE, Epperson CN, Novick AM, Duffy KA, Thompson SM (2024) Beyond the serotonin deficit hypothesis: communicating a neuroplasticity framework of major depressive disorder. Mol Psychiatry 1–12. 10.1038/s41380-024-02625-2
7. Liao C, Dua AN, Wojtasiewicz C, Liston C, Kwan AC (2025) Structural neural plasticity evoked by rapid-acting antidepressant interventions. Nat Rev Neurosci 26:101–114
8. Kopelman J et al (2023) Rapid neuroplasticity changes and response to intravenous ketamine: a randomized controlled trial in treatment-resistant depression. Transl Psychiatry 13:1–9
9. Alagapan S et al (2023) Cingulate dynamics track depression recovery with deep brain stimulation. Nature 622:130–138
10. MacQueen G, Frodl T (2011) The hippocampus in major depression: evidence for the convergence of the bench and bedside in psychiatric research? Mol Psychiatry 16:252–264
11. Mayberg HS (2003) Modulating dysfunctional limbic-cortical circuits in depression: towards development of brain-based algorithms for diagnosis and optimised treatment. Br Med Bull 65:193–207
12. Ding Y-D et al (2022) Reduced nucleus accumbens functional connectivity in reward network and default mode network in patients with recurrent major depressive disorder. Transl Psychiatry 12:1–9
13. Kaiser RH, Andrews-Hanna JR, Wager TD, Pizzagalli DA (2015) Large-Scale Network Dysfunction in Major Depressive Disorder: A Meta-analysis of Resting-State Functional Connectivity. JAMA Psychiatry 72:603
14. Holmes SE et al (2019) Lower synaptic density is associated with depression severity and network alterations. Nat Commun 10:1529
15. Lynch CJ et al (2024) Frontostriatal salience network expansion in individuals in depression. Nature 1–10. 10.1038/s41586-024-07805-2
16. Holz A et al (2019) Enhanced mGlu5 Signaling in Excitatory Neurons Promotes Rapid Antidepressant Effects via AMPA Receptor Activation. Neuron 104:338–352e7
17. Moda-Sava RN et al (2019) Sustained rescue of prefrontal circuit dysfunction by antidepressant-induced spine formation. Science 364:eaat8078
18. Tozzi L et al (2024) A cognitive neural circuit biotype of depression showing functional and behavioral improvement after transcranial magnetic stimulation in the B-SMART-fMRI trial. Nat Ment Health 2:987–998
19. Lowes DC et al (2021) Ventral tegmental area GABA neurons mediate stress-induced blunted reward-seeking in mice. Nat Commun 12:3539

20. Chaudhury D et al (2013) Rapid regulation of depression-related behaviours by control of midbrain dopamine neurons. Nature 493:532–536
21. Pizzagalli DA, Roberts AC (2022) Prefrontal cortex and depression. Neuropsychopharmacology 47:225–246
22. Delli Colli C, Chiarotti F, Campolongo P, Giuliani A, Branchi I (2024) Towards a network-based operationalization of plasticity for predicting the transition from depression to mental health. Nat Ment Health 2:200–208
23. Kuhn M et al (2016) State-Dependent Partial Occlusion of Cortical LTP-Like Plasticity in Major Depression. Neuropsychopharmacology 41:1521–1529
24. Normann C, Schmitz D, Fürmaier A, Döing C, Bach M (2007) Long-term plasticity of visually evoked potentials in humans is altered in major depression. Biol Psychiatry 62:373–380
25. Foy MR, Stanton ME, Levine S, Thompson RF (1987) Behavioral stress impairs long-term potentiation in rodent hippocampus. Behav Neural Biol 48:138–149
26. Tartt AN, Mariani MB, Hen R, Mann JJ, Boldrini M (2022) Dysregulation of adult hippocampal neuroplasticity in major depression: pathogenesis and therapeutic implications. Mol Psychiatry 27:2689–2699
27. Normann C et al (2024) The NMDA receptor subunit GluN2D is a target for rapid antidepressant action. Preprint at. https://doi.org/10.21203/rs.3.rs-4807870/v1
28. Thompson KJ et al (2018) DREADD Agonist 21 Is an Effective Agonist for Muscarinic-Based DREADDs in Vitro and in Vivo. ACS Pharmacol Transl Sci 1:61–72
29. Vestring S, Serchov T, Normann C (2021) Animal Models of Depression - Chronic Despair Model (CDM). J Vis Exp 62579. 10.3791/62579
30. Serchov T et al (2015) Increased Signaling via Adenosine A1 Receptors, Sleep Deprivation, Imipramine, and Ketamine Inhibit Depressive-like Behavior via Induction of Homer1a. Neuron 87:549–562
31. Sarrazin DH et al (2024) Prefrontal cortex molecular clock modulates development of depression-like phenotype and rapid antidepressant response in mice. Nat Commun 15:7257
32. Alboni S et al (2017) Fluoxetine effects on molecular, cellular and behavioral endophenotypes of depression are driven by the living environment. Mol Psychiatry 22:552–561
33. Kupferberg A, Bicks L, Hasler G (2016) Social functioning in major depressive disorder. Neurosci Biobehav Rev 69:313–332
34. Kirchner L et al (2025) Social expectations in depression. Nat Rev Psychol 4:20–34
35. Alfarez DN, Joëls M, Krugers HJ (2003) Chronic unpredictable stress impairs long-term potentiation in rat hippocampal CA1 area and dentate gyrus in vitro. Eur J Neurosci 17:1928–1934
36. Rubio FJ et al (2013) Long-term fluoxetine treatment induces input-specific LTP and LTD impairment and structural plasticity in the CA1 hippocampal subfield. Front Cell Neurosci 7:66

37. Mathis A et al (2018) DeepLabCut: markerless pose estimation of user-defined body parts with deep learning. Nat Neurosci 21:1281–1289
38. Fanselow MS, Dong H-W (2010) Are the Dorsal and Ventral Hippocampus Functionally Distinct Structures? Neuron 65:7–19
39. Fremeau RT et al (2004) Vesicular Glutamate Transporters 1 and 2 Target to Functionally Distinct Synaptic Release Sites. Science 304:1815–1819
40. Herzog E, Takamori S, Jahn R, Brose N, Wojcik SM (2006) Synaptic and vesicular co-localization of the glutamate transporters VGLUT1 and VGLUT2 in the mouse hippocampus. J Neurochem 99:1011–1018
41. Vertes RP, Hoover WB, Szigeti-Buck K, Leranth C (2007) NUCLEUS REUNIENS OF THE MIDLINE THALAMUS: LINK BETWEEN THE MEDIAL PREFRONTAL CORTEX AND THE HIPPOCAMPUS. Brain Res Bull 71:601–609
42. Cassel J-C et al (2013) The reuniens and rhomboid nuclei: neuroanatomy, electrophysiological characteristics and behavioral implications. Prog Neurobiol 111:34–52
43. Holmes SE et al (2022) Imaging the effect of ketamine on synaptic density (SV2A) in the living brain. Mol Psychiatry 27:2273–2281
44. Kavalali ET, Monteggia LM (2020) Targeting Homeostatic Synaptic Plasticity for Treatment of Mood Disorders. Neuron 106:715–726
45. Yun S et al (2018) Stimulation of entorhinal cortex-dentate gyrus circuitry is antidepressive. Nat Med 24:658–666
46. Giannotti G, Heinsbroek JA, Yue AJ, Deisseroth K, Peters J (2019) Prefrontal cortex neuronal ensembles encoding fear drive fear expression during long-term memory retrieval. Sci Rep 9:10709
47. Schmaal L et al (2016) Subcortical brain alterations in major depressive disorder: findings from the ENIGMA Major Depressive Disorder working group. Mol Psychiatry 21:806–812
48. Bremner JD et al (2000) Hippocampal volume reduction in major depression. Am J Psychiatry 157:115–118
49. Czéh B, Simon M, Schmelting B, Hiemke C, Fuchs E (2006) Astroglial plasticity in the hippocampus is affected by chronic psychosocial stress and concomitant fluoxetine treatment. Neuropsychopharmacol Off Publ Am Coll Neuropsychopharmacol 31:1616–1626
50. Roddy DW et al (2019) The Hippocampus in Depression: More Than the Sum of Its Parts? Advanced Hippocampal Substructure Segmentation in Depression. Biol Psychiatry 85:487–497
51. Nestler EJ (2015) Role of the Brain's Reward Circuitry in Depression: Transcriptional Mechanisms. Int Rev Neurobiol 124:151–170
52. Bloodgood BL, Sharma N, Browne HA, Trepman AZ, Greenberg ME (2013) The activity-dependent transcription factor NPAS4 regulates domain-specific inhibition. Nature 503:121–125
53. Peebles CL et al (2010) Arc regulates spine morphology and maintains network stability in vivo. *Proc. Natl. Acad. Sci. U. S. A.* 107, 18173–18178

54. Halasy K, Hajszan T, Kovács ÉG, Lam T-T, Leranth C (2004) Distribution and origin of vesicular glutamate transporter 2-immunoreactive fibers in the rat hippocampus. Hippocampus 14:908–918
55. Vertes RP, Hoover WB, Valle D, Sherman AC, A., Rodriguez J (2006) j. Efferent projections of reuniens and rhomboid nuclei of the thalamus in the rat. J Comp Neurol 499:768–796
56. Goswamee P, Leggett E, McQuiston AR (2021) Nucleus Reuniens Afferents in Hippocampus Modulate CA1 Network Function via Monosynaptic Excitation and Polysynaptic Inhibition. Front Cell Neurosci 15:660897
57. Varela C, Kumar S, Yang JY, Wilson MA (2014) Anatomical substrates for direct interactions between hippocampus, medial prefrontal cortex, and the thalamic nucleus reuniens. Brain Struct Funct 219:911–929
58. Hoover WB, Vertes RP (2007) Anatomical analysis of afferent projections to the medial prefrontal cortex in the rat. Brain Struct Funct 212:149–179
59. Aleksandrova LR, Wang YT, Phillips AG (2020) Ketamine and its metabolite, (2R,6R)-HNK, restore hippocampal LTP and long-term spatial memory in the Wistar-Kyoto rat model of depression. Mol Brain 13:92
60. Duman RS, Malberg J, Thome J (1999) Neural plasticity to stress and antidepressant treatment. Biol Psychiatry 46:1181–1191
61. Turner VS, O'Sullivan RO, Kheirbek MA (2022) Linking external stimuli with internal drives: A role for the ventral hippocampus. Curr Opin Neurobiol 76:102590
62. Ciocchi S, Passecker J, Malagon-Vina H, Mikus N, Klausberger T (2015) Selective information routing by ventral hippocampal CA1 projection neurons. Science 348:560–563
63. Oleksiak CR et al (2021) Ventral hippocampus mediates the context-dependence of two-way signaled avoidance in male rats. Neurobiol Learn Mem 183:107458
64. Muir J et al (2020) Ventral Hippocampal Afferents to Nucleus Accumbens Encode Both Latent Vulnerability and Stress-Induced Susceptibility. Biol Psychiatry 88:843–854
65. Cassel J-C et al (2021) The reuniens and rhomboid nuclei of the thalamus: A crossroads for cognition-relevant information processing? Neurosci Biobehav Rev 126:338–360
66. Ratigan HC, Krishnan S, Smith S, Sheffield ME (2023) J. A thalamic-hippocampal CA1 signal for contextual fear memory suppression, extinction, and discrimination. Nat Commun 14:6758
67. Xu W, Südhof TC (2013) A Neural Circuit for Memory Specificity and Generalization. Science 339:1290–1295
68. Kafetzopoulos V et al (2018) The nucleus reuniens: a key node in the neurocircuitry of stress and depression. Mol Psychiatry 23:579–586
69. der Weel MJD-V, Silva FHL da, Witter MP (1997) Nucleus Reuniens Thalami Modulates Activity in Hippocampal Field CA1 through Excitatory and Inhibitory Mechanisms. *J. Neurosci.* 17, 5640–5650
70. Yang Y, Ju W, Zhang H, Sun L (2018) Effect of Ketamine on LTP and NMDAR EPSC in Hippocampus of the Chronic Social Defeat Stress Mice Model of Depression. Front Behav Neurosci. 12

71. Eichenbaum H (2017) Prefrontal–hippocampal interactions in episodic memory. Nat Rev Neurosci 18:547–558
72. Carreno FR et al (2016) Activation of a ventral hippocampus–medial prefrontal cortex pathway is both necessary and sufficient for an antidepressant response to ketamine. Mol Psychiatry 21:1298–1308
73. Graham K, Spruston N, Bloss EB (2021) Hippocampal and thalamic afferents form distinct synaptic microcircuits in the mouse infralimbic frontal cortex. Cell Rep 37:109837
74. Chen M et al (2024) Brain region–specific action of ketamine as a rapid antidepressant. Science 385:eado7010
75. Yang Y et al (2018) Ketamine blocks bursting in the lateral habenula to rapidly relieve depression. Nature 554:317–322
76. Hu H, Cui Y, Yang Y (2020) Circuits and functions of the lateral habenula in health and in disease. Nat Rev Neurosci 21:277–295
77. Quiroz C et al (2016) Local Control of Extracellular Dopamine Levels in the Medial Nucleus Accumbens by a Glutamatergic Projection from the Infralimbic Cortex. J Neurosci 36:851–859
78. Yu X, Jembere F, Takehara-Nishiuchi K (2022) Prefrontal projections to the nucleus reuniens signal behavioral relevance of stimuli during associative learning. Sci Rep 12:11995
79. Friedman NP, Robbins TW (2022) The role of prefrontal cortex in cognitive control and executive function. Neuropsychopharmacology 47:72–89
80. Diniz CRAF, Crestani AP (2023) The times they are a-changin': a proposal on how brain flexibility goes beyond the obvious to include the concepts of upward and downward to neuroplasticity. Mol Psychiatry 28:977–992
81. Joëls M, Baram TZ (2009) The neuro-symphony of stress. Nat Rev Neurosci 10:459–466
82. Coenen VA et al (2019) Superolateral medial forebrain bundle deep brain stimulation in major depression: a gateway trial. Neuropsychopharmacol Off Publ Am Coll Neuropsychopharmacol 44:1224–1232
83. Henn MC et al (2024) A systematic review of focused ultrasound for psychiatric disorders: current applications, opportunities, and challenges. Neurosurg Focus 57:E8
84. Normann C et al (2018) Antidepressants Rescue Stress-Induced Disruption of Synaptic Plasticity via Serotonin Transporter–Independent Inhibition of L-Type Calcium Channels. Biol Psychiatry 84:55–64
85. Berg S et al (2019) ilastik: interactive machine learning for (bio)image analysis. Nat Methods 16:1226–1232
86. Sherathiya VN, Schaid MD, Seiler JL, Lopez GC, Lerner TN (2021) GuPPy, a Python toolbox for the analysis of fiber photometry data. Sci Rep 11:24212

Figures

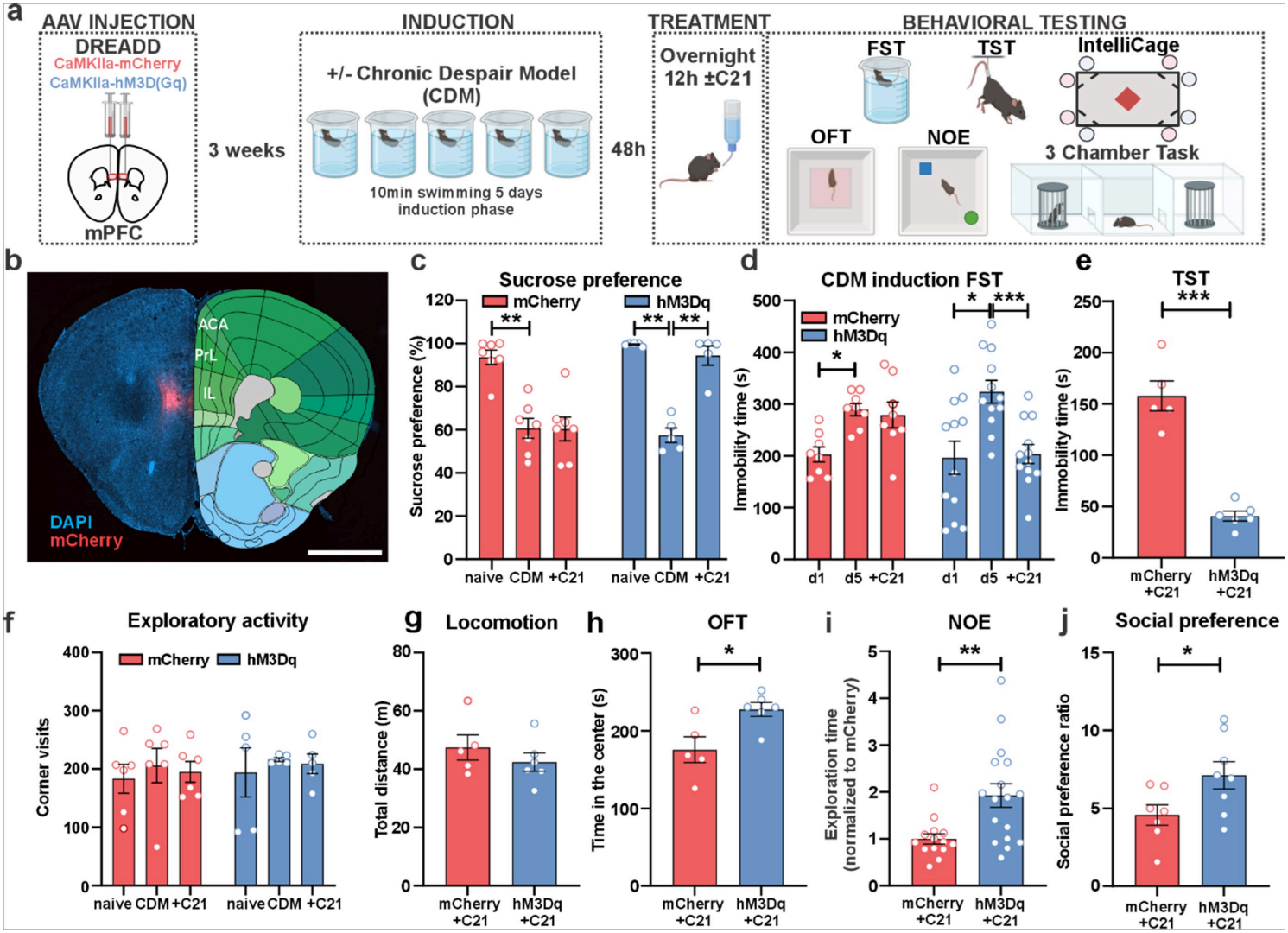

Figure 1

Prefrontal IL DREADDs stimulation produces antidepressant-like effect in various behavioral paradigms. **a** Schematic overview of the experimental design: CaMKIIa-hM3D(Gq) active DREADDs virus or CaMKIIa-mCherry control virus were stereotactically bilaterally injected in IL part of the mPFC. After three weeks rest, a depressive-like state was induced using the chronic despair model (CDM) paradigm (5 days of 10 min swimming). 48 hours later, mice received overnight C21 (0.75mg/kg) in drinking water and were tested in the corresponding behavioral regiment. **b** Representative image of AAV-CaMKIIa-hM3D(Gq)-mCherry injection in the lateral portion of the IL. Scale bar: 1000 µm. **c** Sucrose preference measured in IntelliCage of naïve control, CDM and overnight C21 treated mCherry (n=7) and hM3Dq-injected (n=5) (repeated measures two-way ANOVA with Bonferroni post-hoc test). **d** Immobility time in CDM paradigm from day 1 to day 5 and after overnight treatment with C21 of mCherry (n=8) and hM3Dq (n=12) mice (repeated measures two-way ANOVA with Bonferroni post-hoc test). **e** Immobility time in tails suspension test (TST) (hM3Dq n=6; mCherry n=5, *P*=0.0007, unpaired Welch's t-test). **f** Global exploratory activity measured by corner visits in IntelliCage (mCherry: n=6, hM3Dq: n=5, repeated measures ANOVA with Bonferroni post-hoc test). **g** Locomotion measured by distance travelled in open field test (OFT) of mCherry (n=5) and hM3Dq mice (n=6) (*P*=0.3634, unpaired Student's t-test). **h**Time spent in the central

zone of OFT of hM3Dq-injected mice (n=6) compared to mCherry controls (n=5) (*P*=0.0183, unpaired Student's t-test). **i** Exploratory behavior measured by total time spent exploring two novel objects in novel object exploration (NOE) (mCherry n=14, hM3Dq n=17, *P*=0.0027, Welch's t-test). Data normalized to control group; **j** Social preference measured as time spent exploring a caged visitor mouse divided by time spent exploring a novel object in three-chamber task (mCherry n=7, hM3Dq n=8, *P*=0.0415, unpaired Student's t-test). Data are presented as mean ±SEM and the individual data points are depicted. *P<0.05, **P<0.01, ***P<0.001; See also Supplementary Fig. 1 and Supplementary Fig. 2. Source data are provided as a Source Data file.

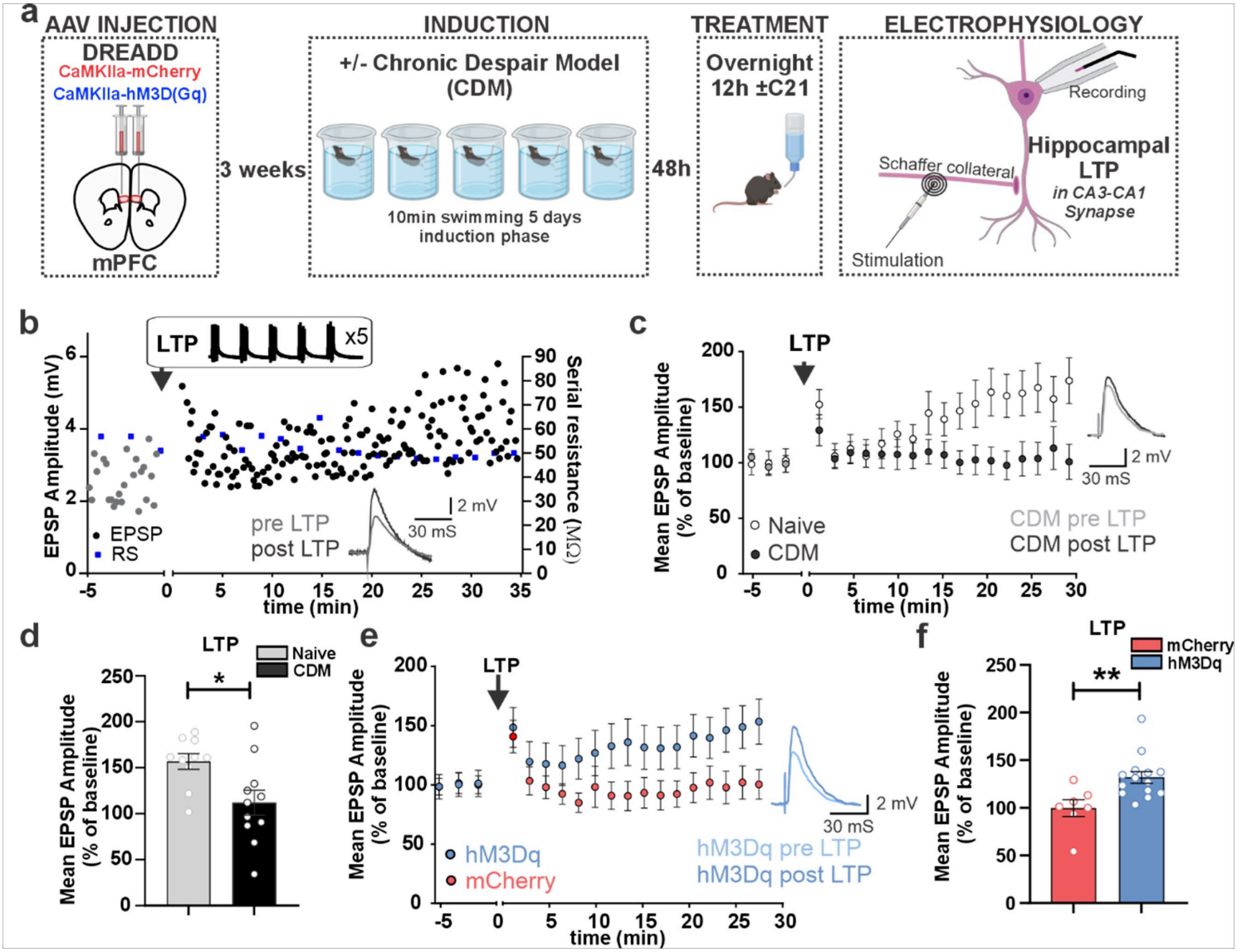

Figure 2

Prefrontal IL DREADDs rescues CDM induced deficits in associative plasticity. a Experimental design: CaMKIIa-HM3D(Gq) active DREADDs virus or CaMKIIa-mCherry control virus were stereotactically bilaterally injected in IL part of the mPFC. After three weeks rest, a depressive-like state was induced using the CDM paradigm (5 days of 10 min swimming). 48 hours later, mice received overnight C21 (0.75mg/kg) in drinking water; mice were then sacrificed for electrophysiology experiments. **b**

Representative aLTP experiment. Each grey dot represents the EPSP amplitudes before an LTP induction protocol (125 EPSP→AP pairings in TBS frequency (upper inset)) and each black dot after the induction protocol. Blue squares represent the serial resistance throughout the experiment. Please note the increase of the exemplary EPSP traces from before (grey trace) to 30 min after the LTP induction protocol (black trace). **c** Left: time course of aLTP inducibility comparing CDM (black) and naive (white). Right: exemplary EPSP trace. **d** Group analysis (naive: n=10, CDM: n=11, *P*=0.0135, Student's t-test). **e** Left: time course of aLTP inducibility after overnight DREADDs activation. Right: exemplary EPSP traces from an hM3Dq injected mouse treated with C21. **f** Group analysis (mCherry n=7, hM3Dq n=14, *P*=0.0023, Mann-Whitney test). Data are presented as mean ±SEM and the individual data points are depicted. **P*<0.05, ***P*<0.01, ***P<0.001. See also Supplementary Fig. 3. Source data are provided as a Source Data file.

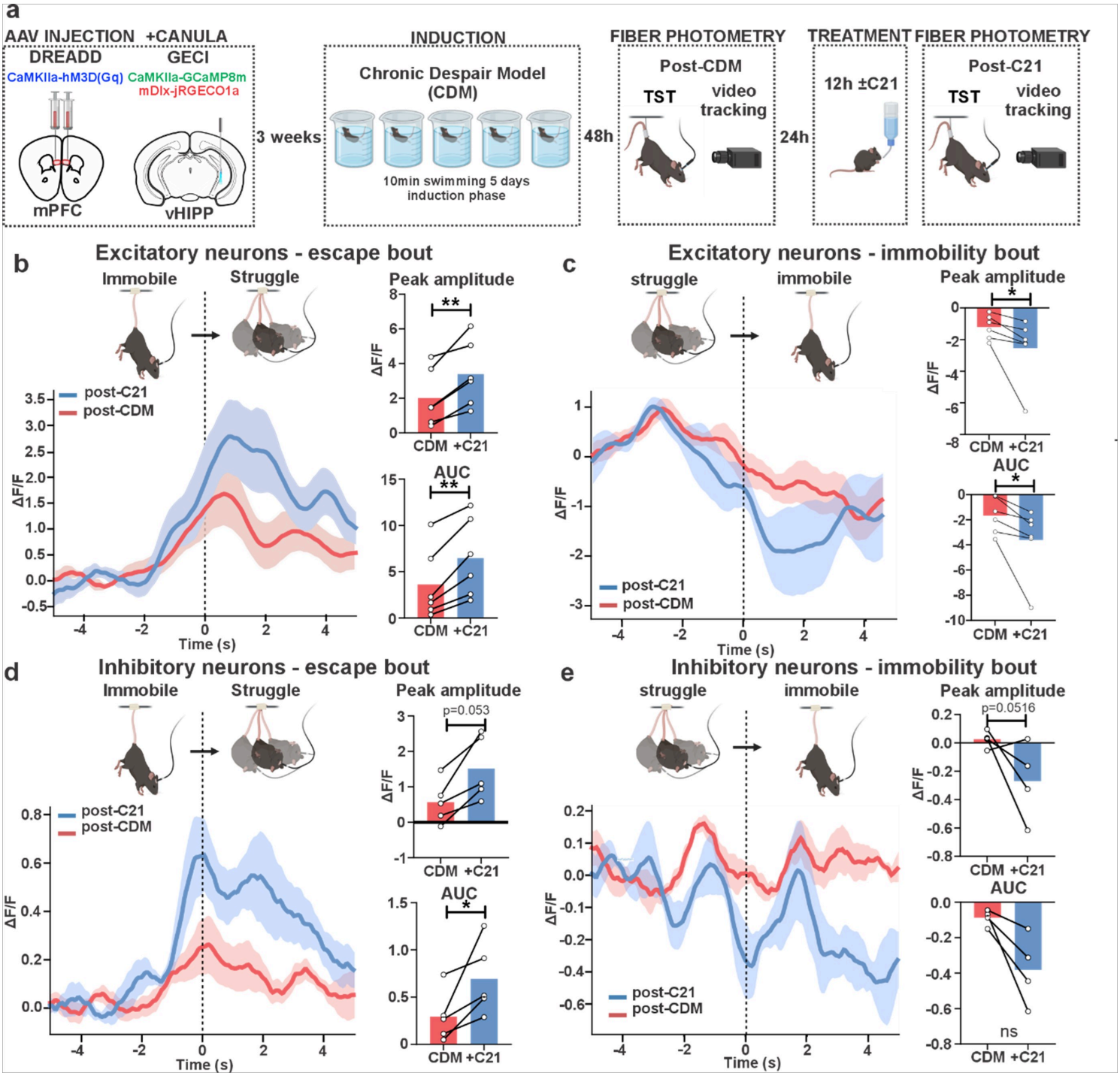

Figure 3

State-dependent modulation of hippocampal circuit dynamics following IL activation. a Experimental design: CaMKIIa-HM3D(Gq) active DREADDs virus was bilaterally injected in the IL, and a calcium indicator targeting excitatory (CaMKIIa-GCaMP8m) or inhibitory (mDlx-jRGECO1a) neurons was virally expressed unilaterally in the ventral hippocampus along with implantation of a fiber optic cannula for photometry recordings. After three weeks of recovery, depressive-like state was induced using the CDM paradigm. 48 hours later, fiber photometry was recorded during TST. 24 hours later, mice received C21 overnight (0.75 mg/kg) followed by a second photometry session. **b** Effect of IL stimulation on excitatory neurons during struggle initiation in TST. Left: Average calcium dynamics (ΔF/F) of hippocampal

excitatory neurons aligned to behavioral state transitions (immobile to struggle) in mice after CDM (post-CDM, red) and following chemogenetic activation of PFC neurons (post-C21, blue). Shaded areas represent SEM. Right: Quantification of peak amplitude and area under the curve (AUC) during the transition period (±5 s) (n=6 mice per group; peak amplitude: P=0.0044; AUC: P=0.0036; paired Student's t-test). **c**Effect of PFC stimulation on hippocampal excitatory neuron activity during transitions to passive behavioral states. Left: Average calcium dynamics (ΔF/F) aligned to transitions from active (struggle) to passive (immobile) states after CDM (post-CDM, red) and following PFC activation (post-C21, blue). Shaded areas represent SEM. Right: Quantification of peak amplitude and AUC (n=6 mice per group; peak amplitude: P=0.0312; AUC: P=0.0312; Wilcoxon matched-pairs signed rank test). **d** Effect of PFC stimulation on hippocampal inhibitory neuron responses during transitions to active behavioral states. Left: Average calcium dynamics (ΔF/F) of hippocampal inhibitory neurons aligned to transitions period after CDM (post-CDM, red) and following PFC activation (post-C21, blue). Shaded areas represent SEM. Right: Quantification of peak amplitudes (P=0.0534) and AUC (P=0.0178) (n=5 mice per group, paired Student's t-test). **e** Calcium dynamics of hippocampal inhibitory neurons during transitions from active to passive states. Left: Average ΔF/F traces aligned to behavioral state transitions after CDM (post-CDM, red) and following PFC activation (post-C21, blue). Shaded areas represent SEM. Right: Quantification of peak amplitude (P=0.0516) and AUC (P=0.1569) during the transition period (n=4 mice per group; paired Student's t-test). Data are presented as mean ±SEM with individual data points shown. P<0.05, *P<0.01, **P<0.001. See also Supplementary Fig. 4. Source data are provided as a Source Data file.

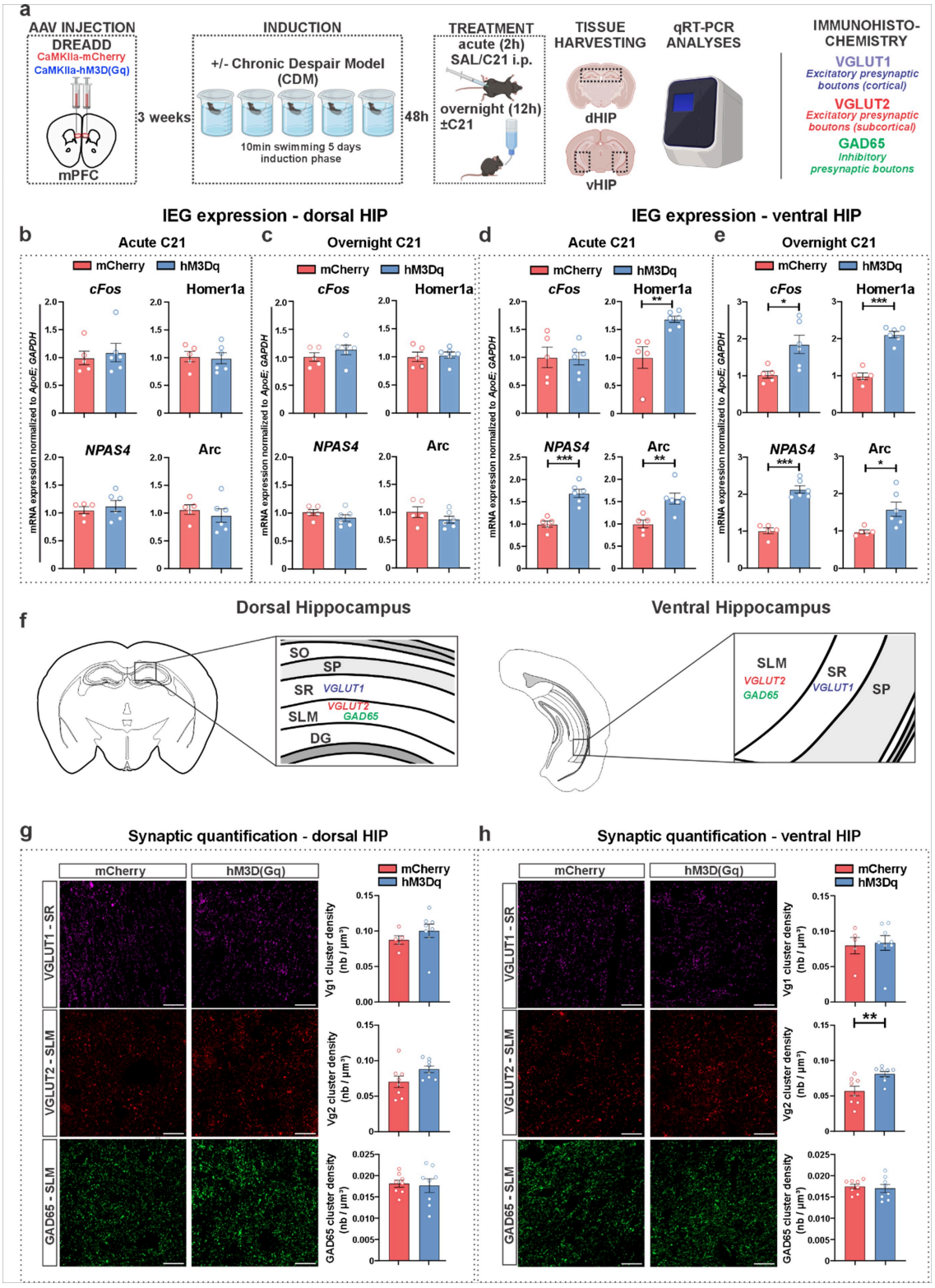

Figure 4

Prefrontal IL DREADD activation differentially regulates immediate early genes and structural synaptic plasticity across hippocampal subregions. a Experimental design. Left: Stereotactic delivery of excitatory DREADD virus (CaMKIIa-hM3D(Gq)) or control virus (CaMKIIa-mCherry) into IL PFC. Middle: After three weeks of recovery, mice underwent CDM consisting of 10-minute swimming sessions for 5 consecutive days. Right: 48 hours after CDM, mice received acute (0.75 mg/kg, i.p) or overnight (0.75mg/kg, drinking

water) C21 treatment followed by tissue collection for qRT-PCR analyses or immunohistochemistry. **b-e**mRNA expression of immediate early genes (normalized to ApoE and GAPDH) of hM3Dq (n=6) and mCherry (n=5) mice in dHIP after acute C21 treatment (*cFos P*=0.6627, *Homer1a P*=0.8339, *NPAS4 P*=0.5610, *Arc P*=0.5108) (**b**) and following overnight C21 treatment (*cFos P*=0.3050, *Homer1a P*=0.7624, *NPAS4 P*=0.2536, *Arc P*=0.2482) (**c**) and in vHIP following acute C21 treatment (*cFos P*=0.0184, *Homer1a P*<0.0001, *NPAS4 P*<0.0001, *Arc P*=0.0243, Welch's t-test) **(d)** and after overnight C21 treatment (*cFos P*=0.9172, *Homer1a P*=0.0043, Mann-Whitney test, *NPAS4 P*=0.0003, *Arc P*=0.0064) (**e**). **f** Schematic representation of dorsal (left) and ventral (right) hippocampal organization. Insets show magnified schematics of hippocampal layers where synaptic density was analysed. VGLUT1-positive clusters were quantified in Stratum Radiatum (SR), while VGLUT2 and GAD65-positive clusters were quantified in Stratum Lacunosum-Moleculare (SLM). SO: stratum oriens; SP: stratum pyramidale; DG: Dentate Gyrus. **g** Synaptic density analysis in CA1 dHIP layers. Left: representative confocal images showing VGLUT1, VGLUT2 and GAD65 immunostaining in SR and SLM of mCherry and hM3Dq mice after overnight C21 treatment. Scale bar: 20µm. Right: Quantification of VGLUT1, VGLUT2 and GAD65 cluster density in hM3Dq and control mice (VGLUT1: mCherry n=5, hM3Dq n=8, *P*=0.1362; VGLUT2: n=8, *P*=0.0809; GAD65: n=8, *P*=0.8055). **h** Synaptic density analysis in CA1 vHIP layers. Left: representative confocal images. Scale bar: 20 µm. Right: Quantification of presynaptic markers in hM3Dq and control mice treated with C21 overnight (VGLUT2: n=8, *P*=0.0081; GAD65: n=8, *P*=0.6843; VGLUT1: mCherry n=5, hM3Dq n=8, *P*=0.3278). Unless otherwise stated, statistical comparisons were performed using unpaired two-tailed Student's t-test. Data are presented as mean ±SEM with individual data points shown. *P*<0.05, **P*<0.01, ***P*<0.001. See also Supplementary Fig. 5. Source data are provided as a Source Data file.

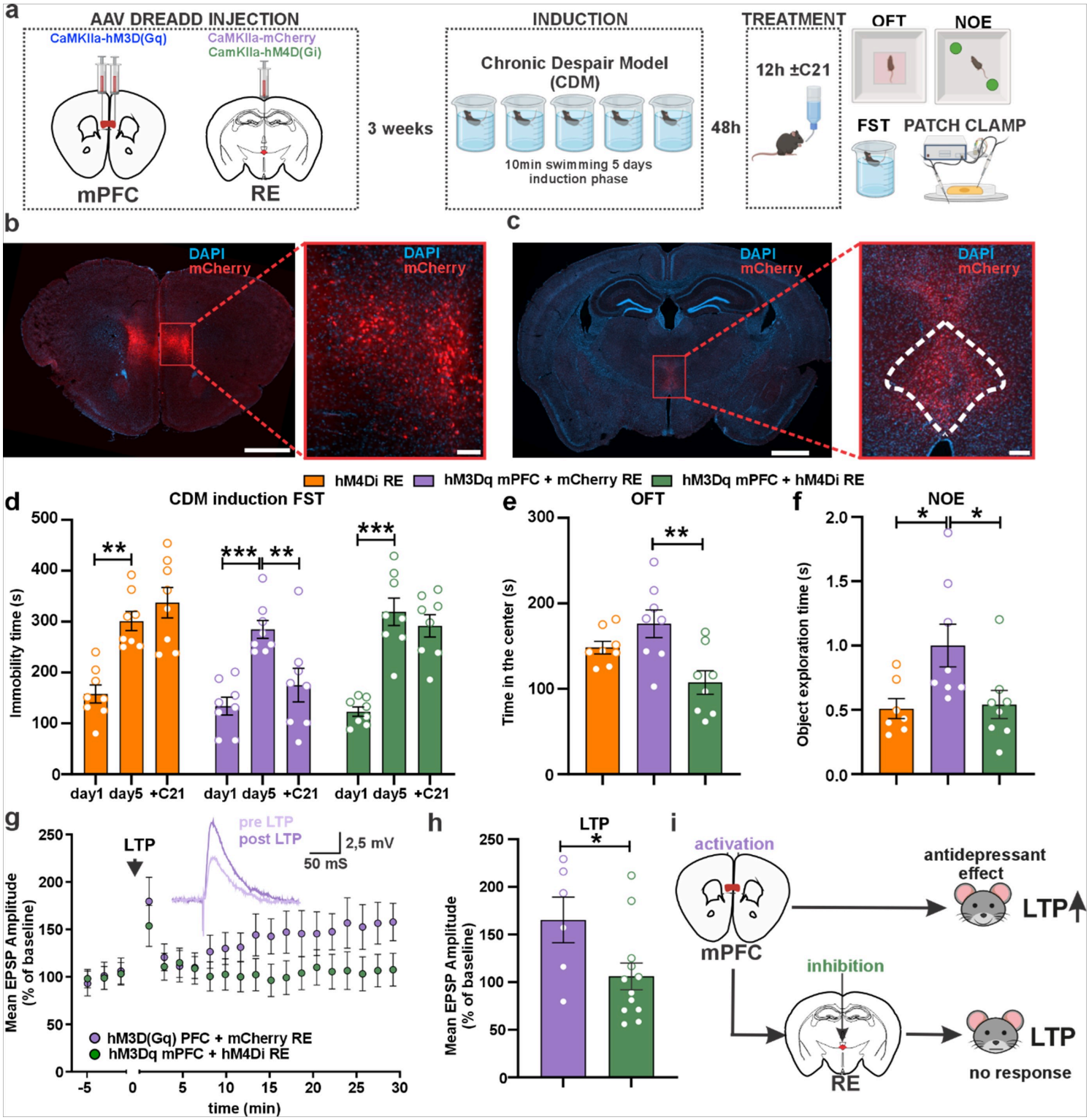

Figure 5

The RE gates IL-stimulation mediated antidepressant effects. a Schematic overview of the experimental design. Stereotactic bilateral delivery of excitatory DREADD virus (CaMKIIa-hM3D(Gq)) in IL and/or inhibitory DREADD (CaMKIIa-hM4D(Gi)) or control virus (CaMKIIa-mCherry) in the Reuniens Nucleus (RE). After three weeks of recovery, mice underwent CDM paradigm. 48 hours after the CDM, mice received C21 (12h overnight treatment) followed by behavioral assessment in OFT, NOE, FST, or patch-

clamp recordings. **b** Representative confocal image of the injection in the prefrontal cortex (scale bar: 1000 µm). Inset shows a higher magnification view (scale bar: 100 µm). **c** Representative confocal image of a reuniens injection. Inset shows a higher magnification view of the RE (scale bar: 100 µm). **d**Immobility time in swim test measured on day 1, day 5 of CDM, and after overnight C21 treatment across experimental groups (n=8 mice per group, repeated measures two-way ANOVA with Bonferroni post-hoc test). **e** Time spent in center in the OFT (n=8, one-way ANOVA followed by Tukey's post-hoc test). **f** Novel object exploration time (normalized to hM3Dq mPFC + mCherry RE group) (hM3Dq mPFC + mCherry RE: n=8, hM4Di RE: n=7, hM3Dq mPFC + hM4Di RE: n=8, one-way ANOVA followed by Tukey's post-hoc test). **g**Time course of aLTP measurements with exemplary EPSP traces from an hM3Dq injected mouse. **h**Group analysis of aLTP measurements of hM3Dq mPFC + mCherry RE (n=6) and hM3Dq mPFC + hM4Di RE (n=12) (*P*=0.0372, unpaired Student's t-test). **i** Schematic summary of the results. PFC IL activation leads to an antidepressant effect, and to a full restoration of hippocampal LTP, and chemogenetic inhibition of the RE abolishes both effects. Data are presented as mean ±SEM and the individual data points are depicted. **P*<0.05, ***P*<0.01, ****P*<0.001. See also Supplementary Fig. 6. Source data are provided as a Source Data file.

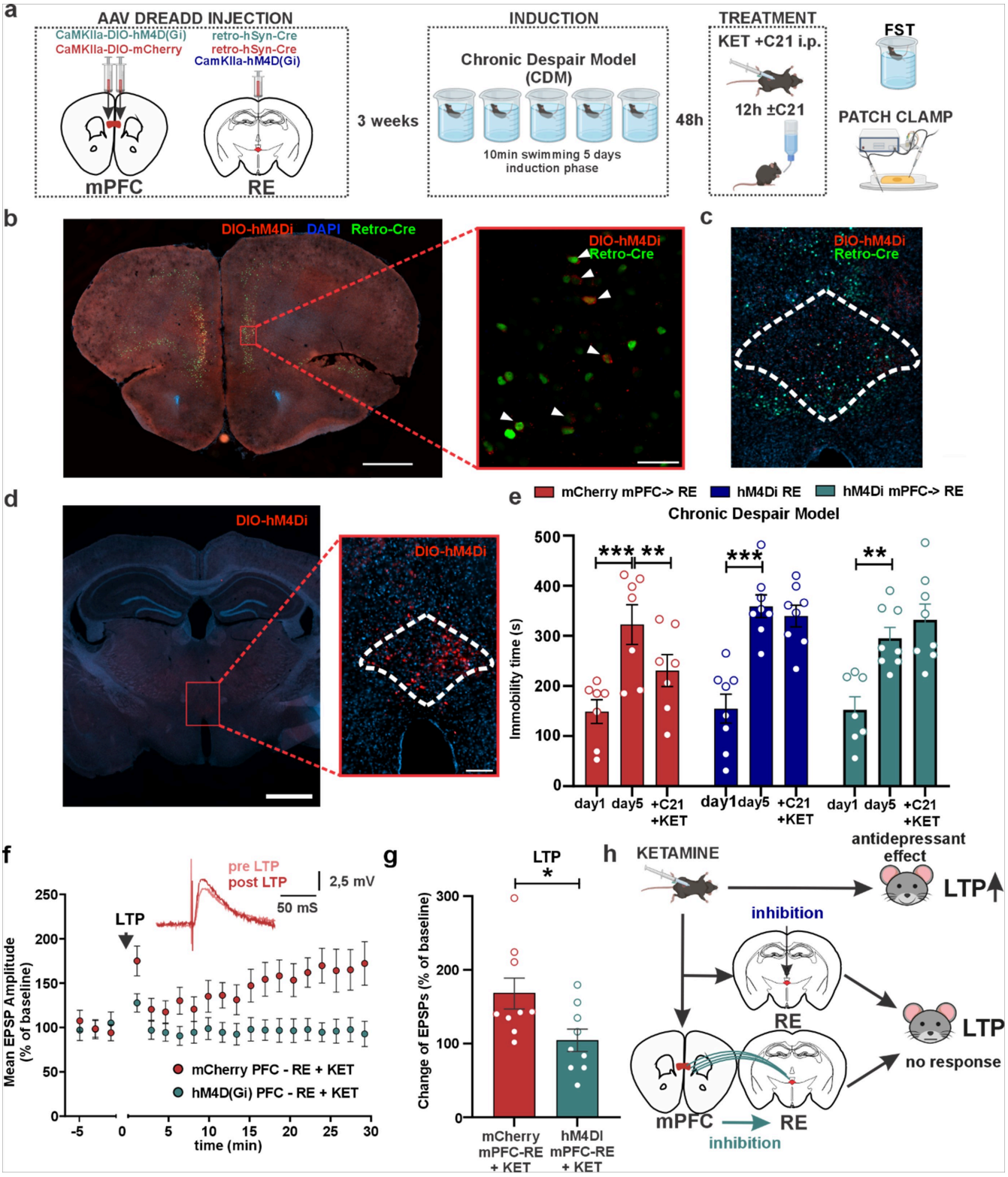

Figure 6

The RE is required for ketamine antidepressant effect and plasticity restoration.

a Schematic overview of the experimental design. Stereotactic bilateral delivery of a retro-hSyn-Cre virus in the RE and CaMKIIa-DIO-hM4D(Gi) or CaMKIIa-DIO-mCherry in IL, or a single delivery of an inhibitory DREADD virus (CaMKIIa-hM4D(Gi)) in the RE. After three weeks of recovery, mice underwent CDM. 48

hours after CDM, mice received ketamine (10 mg/kg) + C21 i.p, and C21 overnight in drinking water, followed by behavioral assessment in FST, or patch-clamp recordings. **b** Representative image of the expression of retro-hSyn-Cre (green) and CaMKIIa-hM4di-mCherry (red) in the IL. Scalebar 1000µm. Inset: higher magnification image of infected cells. Arrowheads indicate double-labelled cells, scalebar 50µm. **c** Representative image of the expression of retro-hSyn-Cre (green) and CaMKIIa-hM4di-mCherry (red) in the RE. Scalebar 100µm. **d**Representative injection of CaMKII-hM4Di virus in the RE, scalebar 1000µm. Inset: zoom in the RE, scalebar 100µm. **e**Immobility time in swim test measured on day 1, day 5 of CDM, and after ketamine treatment (Ketamine + hM4Di RE: n=7; Ketamine + PFC -> RE mCherry: n=8 Ketamine + PFC -> RE hM4Di: n=8; repeated measures two-way ANOVA with Bonferroni post-hoc test). **f-g** Measurements of aLTP between ketamine-treated groups with or without PFC -> RE projection inhibition. **f**Time course of aLTP inducibility of ketamine + mCherry PFC -> RE and ketamine + hM4Di PFC -> RE groups, with exemplary EPSP traces from a PFC -> RE hM4Di injected mouse. **g**Group analysis (n=9, *P*=0.0264, unpaired Student's t-test). **h** Schematic summary of the results. Ketamine 10mg/kg produces antidepressant effect and restores hippocampal aLTP. Chemogenetic blockade of the RE or PFC to RE projections abolishes antidepressant effect and hippocampal aLTP restoration. Data are presented as mean ±SEM and the individual data points are depicted. **P*<0.05, ***P*<0.01, ****P<0.001*. See also Supplementary Fig. 7. Source data are provided as a Source Data file.

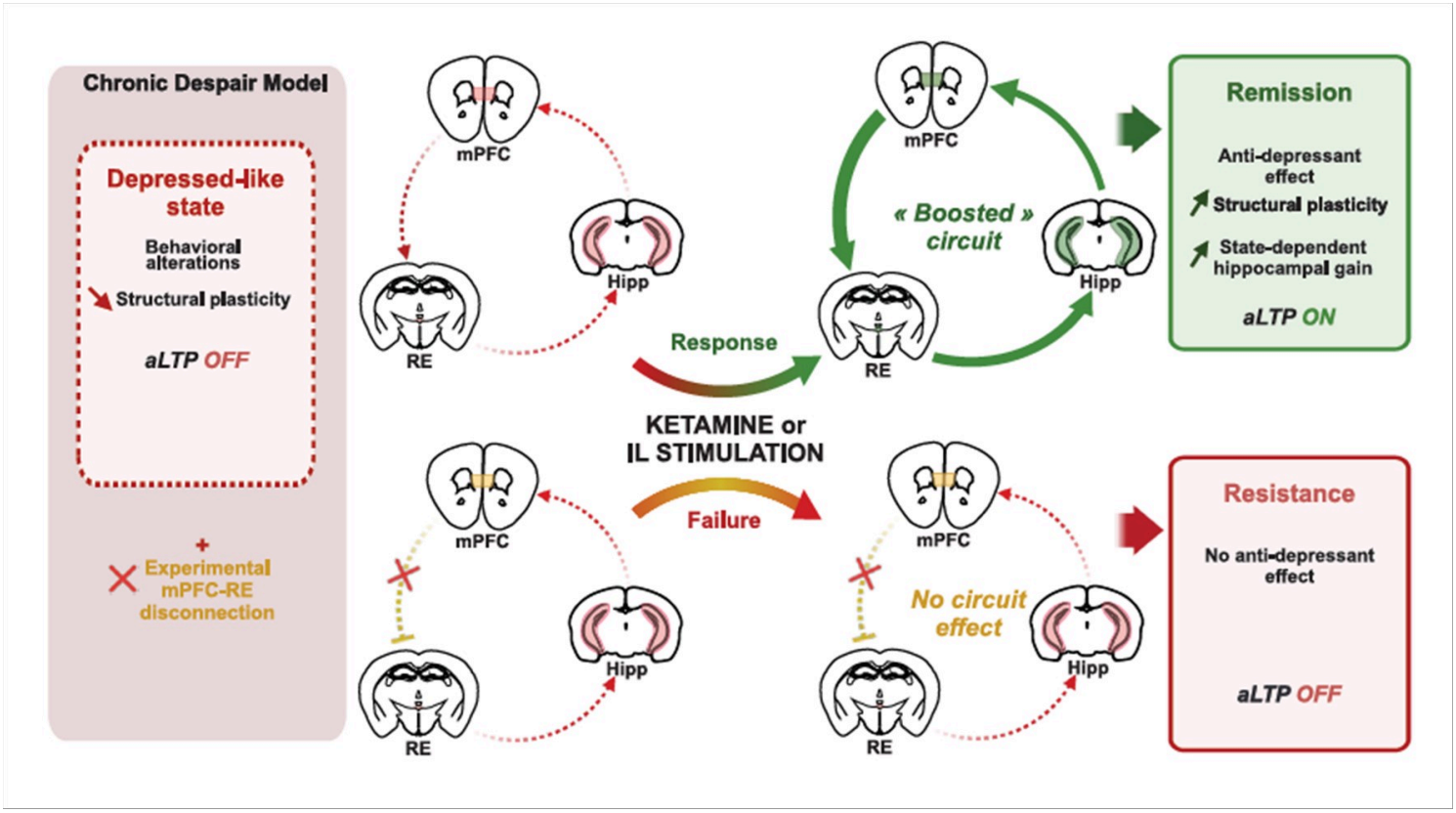

Figure 7

Proposed model for the role of IL → RE → ventral hippocampus → PFC loop in antidepressant response. In a depressed-like state, thecircuit is impaired, and hippocampal aLTP is abolished. Antidepressant treatment using either Ketamine or IL DREADD stimulation activates the circuit, restores normal behavior,

enhances structural plasticity and hippocampal state-dependent dynamics, and rescues aLTP. Conversely, disruption of this loop through the inhibition of mPFC-RE projections prevents the restoration of the circuit, blocking the antidepressant-like effects and the rescue of hippocampal aLTP.

Supplementary Files

This is a list of supplementary files associated with this preprint. Click to download.

- SupplementaryInformations.pdf
- reportingsummary.pdf
- editorialpolicychecklist.pdf
- SourcedataFig1.xlsx
- SourcedataFig2.xlsx
- SourcedataFig3.xlsx
- SourcedataFig4.xlsx
- SourcedataFig5.xlsx
- SourcedataFig6.xlsx
- SourcedataSupplementaryFig1.xlsx
- SourcedataSupplementaryFig2.xlsx
- SourcedataSupplementaryFig3.xlsx
- SourcedataSupplementaryFig4.xlsx
- SourcedataSupplementaryFig5.xlsx
- SourcedataSupplementaryFig6.xlsx
- SourcedataSupplementaryFig7.xlsx